CHAPTER 3

RESULTS

Study 1: Characterization of the key amino acid residues of a single chain variable fragment against HIV-1 matrix protein (MA) or scFv-MA HB-8975 by computational approaches

3.1 Homology modeling of scFv-MA HB-8975

The anti-MA mAb MH-SVM33C9 isolated and characterized by Tewari et al. (1998; 2003) was obtained from ATCC. It is referred to as HB-8975 in ATCC catalog. The amino acid sequence of scFv-MA HB-8975 is shown in **Figure 3.1B**. The order of amino acid was indicated and the Complementarity Determining Regions (CDRs) are underlined using the Kabat method. The V_H and V_L were separately aligned with the immunoglobulin sequences available in Protein Data Bank using BLAST program. The best match for the V_H of scFv-MA HB-8975 was the V_H of idiotype-anti idiotype Fab complex (pdb id: 1iai), sharing 82% of sequence identity with the template, whereas the most homologous V_L of scFv-MA HB-8975 was the V_L of the Fab fragment of a neutralizing antibody directed against an epitope of gp41 from HIV-1 (pdb id: 1nld), sharing 96% of sequence identity with the template. Subsequently, the three dimension structure of scFv-MA HB-8975 was generated based on templates from homology modeling using the MODELLER program as shown in **Figure 3.1A**. In addition, the orientations of the V_H and V_L chains were optimized by superposition using a crystal structure of the anti-DNA binding antibody

(pdb id:2gki) as a scaffold template. To minimize the steric clashes, the 3D structure of scFv-MA HB-8975 was subjected to energy minimization using AMBER03 force field and validation using PROCHECK. As a result, more than 92% of the residues were in the most favored regions of the Ramachandran plot, and overall G-factors were inside the expected regions for structures with 2.0Å resolutions. There are actually six unique hypervariable units in scFv-MA HB-8975 molecule as shown in **Figure 3.1B**. Each of the chains contains three of the six loops that form the binding groove. The hypervariable portions of the loops on the heavy chain are designated H1(31–35), H2(50–66) and H3(99–104) while those on the light chain are L1(154–169), L2(185–190), and L3(224 232) (Tewari et al., 1998). These regions are also known as CDRs, which have a high binding affinity to the antigen.

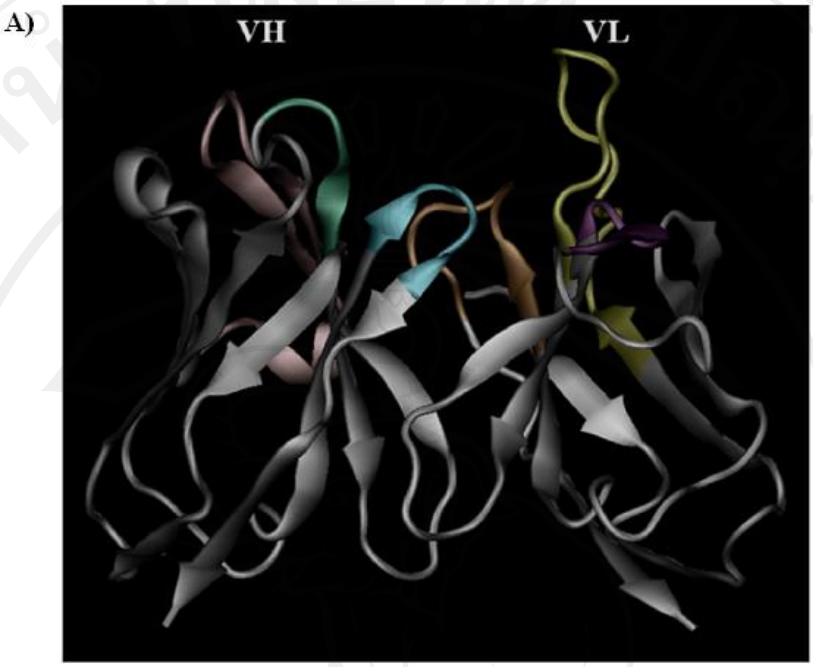

B) VH sequence

CDR H1

QIQLVQSGPELKKPGETVEISCKASGYTFTDYGMNWMKQAPGKSLKWMGW 50

CDR H2

INTYTGEPTYADEFKGRFAFSLETSASTAYLQINNLKSEDMATYFCSRSM 100

CDR H3

KGSYWGQGTLVTVSA 115

VL sequence

CDR L1

DVVMTQTPLTLSVTIGQPASISCKSSQSLLGSDGKTFLNWLLQRPGQSPK 50

CDR L2 CDR L3

RLIYLVSKLDSGVPDRFTGSGSGTDFTLKISRVEAEDLGVYYCWQGTXLP 100

QTFGGGTKLEIK 112

Figure 3.1 Molecular models of scFv-MA HB-8975. (A) The 3D structural model of scFv-MA HB-8975. V_H and V_L domains are colored in white. The hypervariable binding loops are colored in green (H1), pink (H2), cyan (H3), yellow (L1), purple (L2), and orange (L3) respectively. **(B)** Amino acid sequences of the hypervariable binding V_H (1–114) and V_L (131–241) domains of scFv-MA HB-8975; the loops in the heavy chain (CDRH1: 31–35, CDRH2: 50–66, and CDRH3: 99–104), and the loops in the light chain (CDRL1: 154–169, CDRL2: 185-190, and CDRL3: 224–232) of the scFv antibody.

3.2 Evaluation of the scFv-MA HB-8975-peptide complexes by molecular docking

To investigate the binding activity of scFv-MA with nine peptide epitopes by computational study, the scFv-MA HB-8975 antibody with the peptide epitope was assembled and modeled based on a homology modeling approach. The models of scFv-MA HB-8975, nine peptide epitopes, and the scFv-peptide complexes were generated separately. The sequences of mutated peptides that were obtained from the GenBank database comprised the following positions: the single mutation of S126N, V128I, S125N D121N, H124N, V128A, S126K, and the double mutation of H124N and S125N. The sequences of all peptide epitopes that were initially positioned outside the binding region were docked against scFv-MA HB-8975 in the same manner. The PMF scores **(Table 3.1)** of the complex structures were calculated with the BioMedCaChe 2.0 (Fujitsu, Inc.) program, where flexible peptide epitopes were docked into flexible side chain proteins. The peptide epitopes and the side chains of the amino acids of the CDRs were kept flexible during the docking simulation. The PMF scores were in the range of −829.939 to −926.793 kcal/mol. The peptides bound in two orientations, where the N-terminal (p17.1, p17.2, p17.4–p17.6, and p17.8) and the C-terminal (p17.3, p17.7, and p17.9) of peptide sequences were directed toward the binding pocket. All interactions of the optimum docking structures reflected the negative binding energies in all models, indicating favorable binding in all complexes. Less favorable binding of peptide 17.7 and p17.9 to scFv-MA HB-8975 was observed, whereas peptide 17.8 had higher binding energy score. The interacting amino acids of scFv-MA HB-8975 within 4.5Å from an individual docked peptide are

listed in **Table 3.1**. The common binding residues of scFv-MA HB-8975 are composed of the combination of hydrophilic and hydrophobic amino acids: Trp50 (H2), Thr59 (H2), Ser99 (H3), Met100 (H3), Lys101 (H3), Ser103 (H3), Asp163 (L1), Phe167 (L1) Asp190 (L2), Gly226 (L3), Thr227 (L3), His228 (L3), and Leu229 (L3), as indicated in boldface type.

Table 3.1 PMF scores and residues on CDR loops of scFv-MA HB-8975 at 4.5 Å from each of nine peptide epitopes. The common amino acids are in boldface typr

Peptide names	Peptide sequences	PMF score (kcal/mol)	Amino Acid in 4.5 Å from peptide epitope	
			Nonpolar hydrophobic	Polar hydrophilic
p17.1	^{121}DTGHSSQVSQNY^{132}	−902.11	GLY33 (H1), **TRP50 (H2)**, **MET100 (H3)**, **GLY226 (L3)**, **LEU229 (L3)**	**SER99 (H3)**, **SER103 (H3)**, **ASP163 (L1)**, **ASP190 (L2)**, **THR227 (L3)**
p17.2	^{121}DTGHS<u>N</u>QVSQNY^{132}	−899.18	**TRP50 (H2)**, **MET100 (H3)**, GLY161 (L1), LEU185 (L2), **GLY226 (L3)**, **LEU229 (L3)**	**THR59 (H2)**, **SER99 (H3)**, **LYS101 (H3)**, **SER103 (H3)**, SER162 (L1), **ASP163 (L1)**, **THR227 (L3)**, HIS228 (L3)
p17.3	^{121}DTGHSSQ<u>I</u>SQNY^{132}	−882.65	**TRP50 (H2)**, **MET100 (H3)**, PHE167 (L1), **GLY226 (L3)**, **LEU229 (L3)**	**SER99 (H3)**, **LYS101 (H3)**, **ASP163 (L1)**, TYR184, **ASP190 (L2)**, SER191, **THR227 (L3)**, GLN231 (L3)
p17.4	^{121}DTGH<u>N</u>SQVSQNY^{132}	−898.71	GLY33 (H1), **MET100 (H3)**, **GLY226 (L3)**, **LEU229 (L3)**	ASP31 (H1), TYR32 (H1), ASN52 (H2), **SER99 (H3)**, **LYS101 (H3)**, HIS228 (L3), GLN231 (L3)
p17.5	^{121}<u>N</u>TGHSSQVSQNY^{132}	−843.51	**TRP50 (H2)**, **MET100 (H3)**, **PHE167 (L1)**, LEU185 (L2), **LEU229 (L3)**	ASN35 (H1), **SER99 (H3)**, **LYS101 (H3)**, ASN169 (L1), TYR184, **ASP190 (L2)**, SER191, **THR227 (L3)**, **HIS228 (L3)**
p17.6	^{121}DTG<u>N</u>SSQVSQNY^{132}	−846.12	GLY33 (H1), **TRP50 (H2)**, **MET100 (H3)**, **LEU229 (L3)**	**SER99 (H3)**, **LYS101 (H3)**, LYS165 (L1), TYR184, SER191
p17.7	^{121}DTGHSSQ<u>A</u>SQNY^{132}	−829.94	**TRP50 (H2)**, **MET100 (H3)**, **PHE167 (L1)**, **GLY226 (L3)**	**THR59 (H2)**, **LYS101 (H3)**, LYS165 (L1), LYS188 (L2), **THR227 (L3)**, HIS228 (L3)
p17.8	^{121}DTGHS<u>K</u>QVSQNY^{132}	−926.79	**TRP50 (H2)**, **MET100 (H3)**, **PHE167 (L1)**, **GLY226 (L3)**, **LEU229 (L3)**	**THR59 (H2)**, **SER99 (H3)**, **LYS101 (H3)**, **SER103 (H3)**, SER162 (L1), **ASP163 (L1)**, **THR227 (L3)**
p17.9	^{121}DTG<u>NN</u>SQVSQNY^{132}	−841.02	**TRP50 (H2)**, **MET100 (H3)**, **PHE167 (L1)**, LEU185, **LEU229 (L3)**	**THR59 (H2)**, **SER99 (H3)**, **LYS101 (H3)**, LYS165, ASN169 (L1), TYR184, **ASP190 (L2)**, SER191, **HIS228 (L3)**

The underlined letters are the mutated residues in each sequence compared to the wild type.

3.3 Construction of phagemid vector encoding scFv-MA HB-8975

Laboratory experiments were performed to confirm the predicted data from molecular modeling and docking. The DNA encoding scFv-MA HB-8975 fragment was successfully generated from hybridoma cell producing anti-MA HB-8975. Subsequently, the scFv fragment was cloned into a pComb3X-SS phagemid vector resulting in pComb3X-scFv-MA vector as shown in **Figure 3.2.** The scFv-MA HB-8975 construct was combined at the N-terminus with *OmpA* signal sequence for protein transportation and the C-terminus with: His6 and HA tags for detection purpose, amber stop codon (TAG) for soluble protein production, and the minor coat protein, gpIII for surface display on the phage particles, respectively.

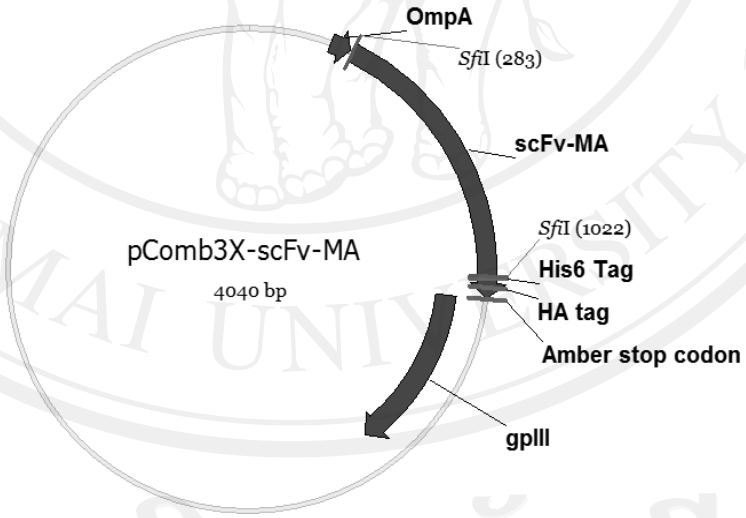

Figure 3.2 Schematic figure of pComb3X-scFv-MA phagemid vector. The scFv-MA HB-8975 fragment was cloned into pComb3X-SS phagemid vector *via Sfi* I restriction site. The scFv-MA HB-8975 was fused with *OmpA* signal sequence at the N-terminal and the C-terminus with; His6 and HA tag, amber stop codon, and the minor coat protein, gpIII, respectively.

3.4 Detection of phage particles displaying scFv-MA HB-8975 and soluble scFv-MA HB-8975

To produce phage pariticles displaying scFv-MA HB-8975, the pComb3X-scFv-MA phagemid vector was transformed into the amber suppressing (supE) *E. coli* strain, XL-1 Blue which read-through of the amber stop codon resulting in scFv-gpIII fusion protein. The bacteria cells harboring pComb3X-scFv-MA phagemid vector were induced to produce protein with IPTG and infected with VCSM13 helper phages. Finally, scFv-MA HB-8975 displayed phage particles were obtained by PEG precipitation and were assessed by immunoblotting using anti-gpIII mAb. The immunoreactive band of scFv-gpIII fusion protein migrated with an apparent molecular weight of approximately 43 kDa **(Figure 3.3A)**, whereas the VCSM13 helper phage only showed the reactive band of wild-type gpIII with molecular weight of approximately 65 kDa. The surface display of scFv-MA HB-8975 on phage particles was therefore successfully constructed.

The non suppressor *E. coli* strain, HB-5121 was used as a host for the expression of soluble scFv-MA HB-8975 protein. The bacteria cells containing pComb3X-scFv-MA were cultured and protein expression was induced with 1 mM IPTG. The soluble protein in the culture supernatant was precipitated by ammonium precipitation and concentrated with Amicon Ultra centrifuge filter. The soluble scFv-MA HB-8975 was separated by SDS-PAGE blot and investigated using anti-HA tag mAb. The reactive band of soluble scFv-MA HB-8975 was observed at approximately 34 kDa **(Figure 3.3B)** indicating that soluble scFv-MA HB-8975 protein was produced by the non suppressor *E. coli* strain, HB5121.

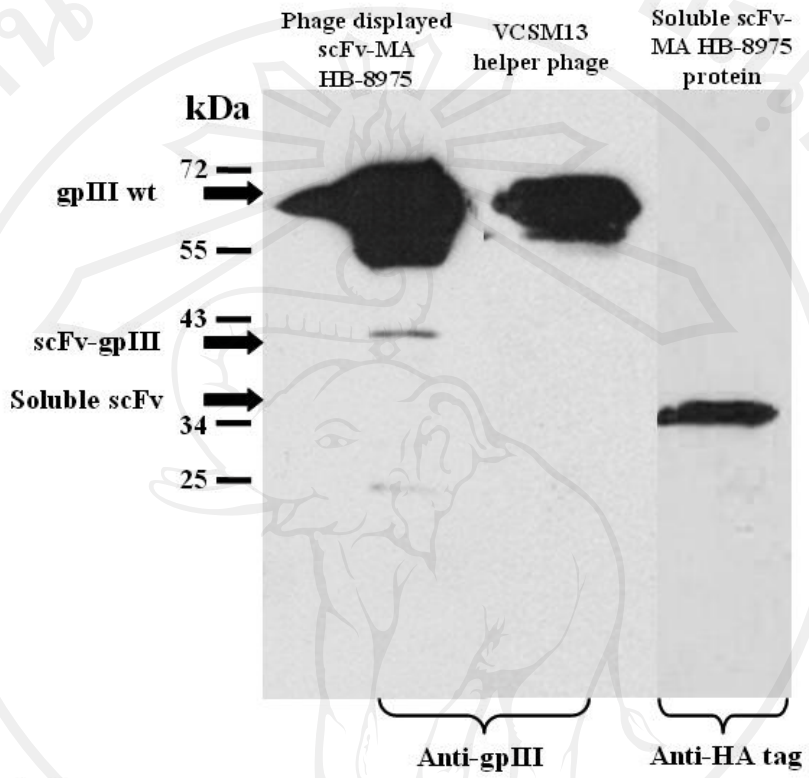

Figure 3.3 Verification of phage displayed scFv-MA HB-8975 and soluble scFv-MA HB-8975. Recombinant phages (10^{12} cfu/ml) and concentrated soluble scFv-MA HB-8975 were separated on a reducing 12% SDS-PAGE. The scFv-gpIII and gpIII wild-type were probed with anti-gpIII mAb while soluble scFv was detected with anti-HA tag mAb. Molecular weight markers in kDa are indicated.

3.5 Characterization of phage-displayed scFv-MA HB-8975 and soluble scFv-MA HB-8975

The binding activity of phage-displayed scFv-MA HB-8975 and soluble scFv-HB-8975 protein were investigated by indirect ELISA using the wild-type peptide epitope p17.1 as an antigen. As shown in **Figure 3.4**, phage-displayed scFv-MA HB-8975 showed a high signal against p17.1, but not VCSM13 helper phage control. In addition, positive signal was also found in soluble scFv-MA HB-8975. The anti-MA mAb HB-8975, positive control, could recognize p17.1 peptide as expected. No significant signal was observed in uncoated well. These results implied that both scFv-MA HB-8975 forms, scFv-gpIII fusion protein and soluble protein, had the same reactivity with p17.1 peptide as that of the parental monoclonal antibody.

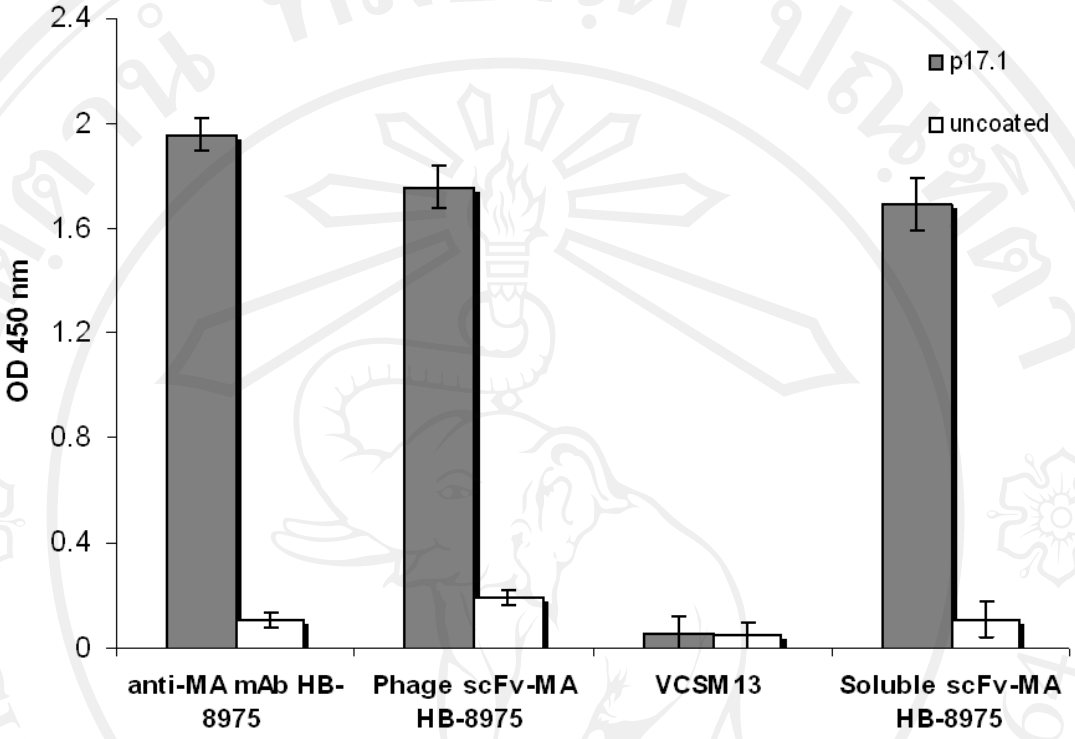

Figure 3.4 Determination of the binding activity of phage-displayed scFv-MA HB-8975 and soluble scFv-MA HB-8975. Wells were coated with p17.1 peptide. 10^9 cfu/ml of phage particles and 200 ug/ml of soluble protein were added and traced by HRP-conjugated anti-M13 mAb and HRP-conjugated anti-HA tag mAb, respectively. The anti-MA mAb HB-8975 was used as a positive control and VCSM13 helper phage was used as wild-type phage control.

3.6 Comparison of calculated binding free energy from computational assisted model and experimental data

According to the PMF score shown in **Table 3.1**, four peptides, one wild-type peptide (p17.1) and three mutant peptides (p17.3, p17.7, and p17.8) were chosen for further investigation by peptide ELISA and MDs. The rationale was that p17.7 had the lowest score and p17.8 had the highest score, whereas p17.3 had very similar score to that of the p17.1 wild-type peptide. The reactivity of phage-displayed scFv-MA HB-8975 and soluble scFv-MA HB-8975 against peptides were demonstrated by peptide ELISA. As shown in **Figure 3.5**, positive signals were observed in all peptide-coated wells, indicating that both recombinant phage particles and soluble protein could bind to all mutant peptides. The peptide p17.8 gave the highest signal followed by p17.1, p17.3 and p17.7, respectively. No signal was detected with irrelevant antigen, CD147 protein, and uncoated wells. Moreover, all soluble mutant peptides were able to inhibit the binding of phage particles and soluble protein to immobilized p17.1 peptide **(Table 3.2)**, as revealed by the percentage of inhibition (PI). By contrast, CD147 protein had no significant inhibitory effect. The peptides p17.1 and p17.8 exhibited the highest inhibitory effects compared to the other two peptides, p17.3 and p17.7, at the same concentration. The high PI indicated the high binding activity. Taken together, both scFv-MA HB-8975 forms specifically reacted with p17 peptides, although the binding activity of individual mutant peptides was different. Their apparent affinity could be ranked as follows: p17.8 > p17.1 > p17.3 > p17.7.

Comparison of the binding data from laboratory experiments with the results derived from molecular docking. Initially, favorable configurations for forming a scFv-antigen complex system were built by molecular docking. To understand the binding interaction in water, the binding free energies of those complexes were simulated by molecular dynamics simulations (MDs), and the Molecular Mechanics Poisson–Boltzmann Surface Area (MM-PBSA) methodology was applied to calculate the binding free energy of all residues of the complexes. The value of PB_{TOT} was used to compare the simulation with the experimental data. The more negative value represented the more favorable binding status. As shown in **Table 3.2**, the binding energies identified by the MM-PBSA protocol were ranked as follows: peptide p17.1 < p17.8 < p17.3 < p17.7 with the values of −29.98, −26.38, −8.82, and −8.77 kcal/mol, respectively. The results were consistent with the percentage of inhibitory value (PI) from competitive ELISA. In addition, the mutant peptides were divided into two groups, with high and low activities, respectively. The binding free energy of scFv with p17.1 and p17.8 peptide represented more negative value, approximately 18 kcal/mol compared to p17.3 peptide. Consequently, the p17.3, p17.7 and p17.9 were identified as the low affinity binding peptides, whereas the p17.1, p17.2, and p17.8 were designated as the high affinity binding peptides. Taken together, the predicted data from computational approach were in good consistency with our experimental data, and demonstrate the binding activity of scFv-MA HB-8975 with HIV-1 MA peptide epitopes and natural mutant variants of the MA peptide epitopes.

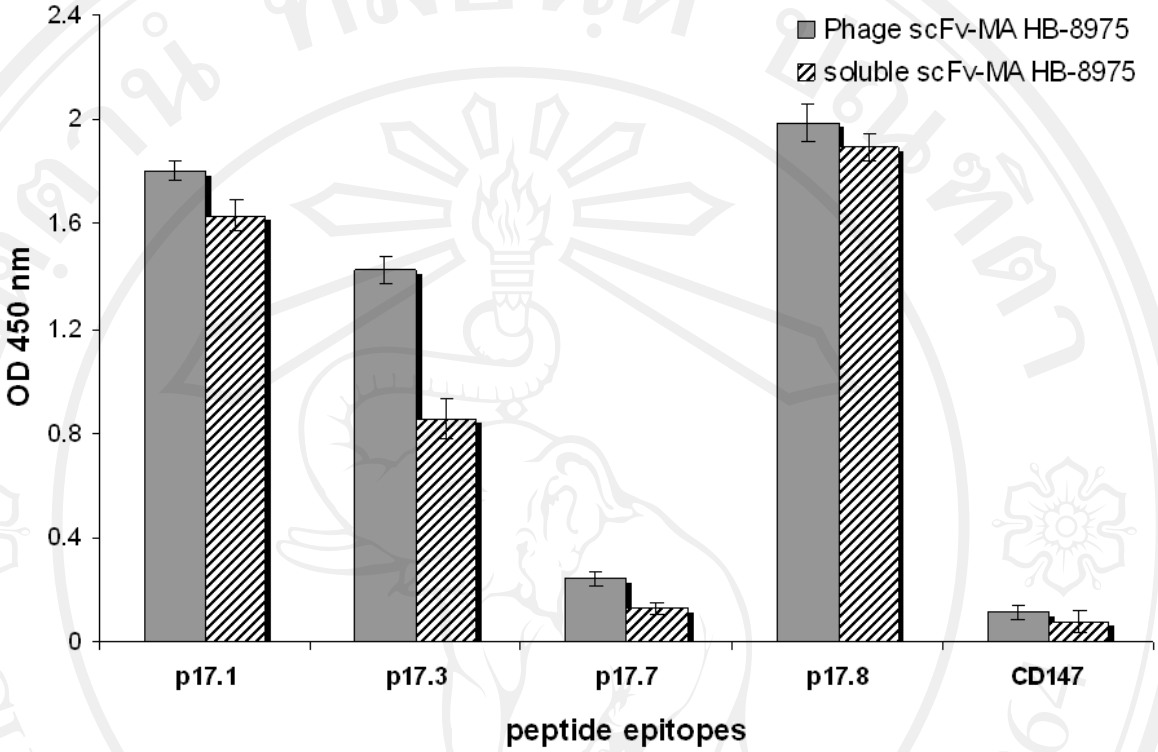

Figure 3.5 Characterization of phage-displayed scFv-MA HB-8975 and soluble scFv-MA HB-8975 with HIV-1 MA mutant/variant peptides. Phage particles at 10^9 cfu/ml and 200 ug/ml of soluble protein were added into each peptide coated wells and traced by HRP-conjugated anti-M13 mAb and HRP-conjugated anti-HA tag mAb, respectively. CD147 protein was used as irrelevant antigen control.

Table 3.2 Relationship between the data of binding activity from competitive ELISA and those from MM-PBSA methodology

Peptide names	Total binging free energy ($\triangle PB_{TOT}$) (kcal/mol)	Experimental value (competitive ELISA:PI (%))	
		Phage-displayed scFv-MA HB-8975	Soluble scFv-MA HB-8975
p17.1	-29.98	62.17	75.94
p17.3	-8.82	45.66	55.24
p17.7	**-8.77**	**29.46**	**44.60**
p17.8	**-26.38**	**67.10**	**79.46**
CD147	-	5.54	7.94

The highest affinity binding peptide, p17.8, and the lowest affinity binding peptide, p17.7, are indicated in bold letters.

3.7 Decomposition of energy on the amino acid residues in CRD and specific contact upon binding

To identify the key residues in the interaction of scFv-MA HB-8975 against HIV-1 MA peptides, decomposition of energy by calculating the binding free energies was measured. The important residues of scFv-MA HB-8975 would show strong interactions in association with its antigen. The calculated data obtained by the MM-PBSA approach and laboratory experiments allowed us to estimate the protein–ligand interactions. The relative decomposition energies of amino acids on the CDRs of scFv-MA HB-8975 versus each of four peptide epitopes were calculated and plotted as shown in **Table 3.3** and **Figure 3.6A**. All amino acids in CDRs of the scFv

sequences were found to exhibit positive or negative influences on binding to the substrate molecules. The superior binding activity in each residue was indicated by the lower decomposed energy with the relative energy below 2 kcal/mol. Several residues of the p17.1 wild-type peptide (Trp50, Met100, Lys101, Phe167, Asn169, Thr227, His228, Leu229 and Gln231) were found to have significant contributions since the absolute relative energy was larger than 2 kcal/mol indicating strong interdependent effects of the individual residues in the epitope sequences. Among three mutated peptides, poor binding and/or weak interaction was obtained from Met100, Lys101, Asn169, His228, and Leu229. The difference between high and low affinity binding depends on the interaction of each peptide with the particular amino acids in the CDR region of scFv. Indeed, the Trp50 of scFv exhibited more interaction with both p17.3 (V128I) and p17.8 (S125K) than the p17.1 wild-type peptide. The Met100, Lys101, Asn169, His228, and Leu229 showed the strongest binding with p17.1 peptide, whereas Try50, Phe167 and Thr227 exhibited the strongest binding with p17.8. There was only one strong binding interaction among other peptides with Gln231 as observed in sequence 17.3 and there was no strong binding interaction with 17.7 which resulted in a low binding affinity. These interactions make a significant contribution to the overall binding. Interestingly, the decomposed energies of some residues in scFv have positive values with peptide epitopes. A particularly strong case, with decomposed energy of 4.24 kcal/mol, was observed for p17.8 binding with Lys101.

Further analysis of the final MD complex structures is shown in **Figure 3.6B**. As expected, p17.7 may bind with different patterns from other peptides since its C-

terminal has binding sites oriented toward the inside of the pocket instead of the N-terminal whereas p17.1, p17.3, and p17.8 demonstrated in different orientation.

Overall we found that Met100(H3), Lys101(H3), Asn169(L1), His228(L3), and Leu229(L3) exhibited strong interactions with peptide p.17.1 **(Figure 3.6B).** The binding activity of scFv-MA HB-8975 with p17.7 peptide was lower than with other peptides because of the reverse orientation of p17.7 peptide in the binding pocket **(Figure 3.6B).**

Table 3.3 Common interacting residues found among the nature peptide sequences in the docking study

Residue	Loop	Decomposed energy (kcal/mol)			
		p17.1	p17.3	p17.7	p17.8
ASP31	H1	0.26	0.35 (0.09)	0.28 (0.02)	0.24 (−0.02)
TYR32	H1	0.04	−0.05 (−0.09)	0.03 (−0.01)	0.01 (−0.03)
GLY33	H1	0.01	−0.08 (−0.09)	−0.02 (−0.03)	−0.11 (−0.12)
ASN35	H1	0.14	−0.14 (−0.28)	−0.09 (−0.23)	−0.34 (−0.48)
TRP50	H2	−1.73	**−3.76 (−2.03)**	−2.05 (−0.32)	**−4.90 (−3.17)**
ASN52	H2	0.03	−0.25 (−0.28)	−0.05 (−0.08)	−0.84 (−0.87)
THR59	H2	0.04	−0.56 (−0.60)	−0.57 (−0.61)	−0.61 (−0.65)
SER99	H3	−0.18	−0.17 (0.01)	0.09 (0.27)	−0.62 (−0.44)
MET100	H3	−3.80	**−1.02 (2.78)**	−3.27 (0.53)	−3.59 (0.21)
LYS101	H3	−2.91	**−0.56 (2.35)**	−1.10 (1.81)	**4.24 (7.15)**
SER103	H3	−0.11	0.06 (0.17)	0.03 (0.14)	−1.31 (−1.2)
GLY161	L1	0.01	−0.01 (−0.02)	−0.07 (−0.08)	−0.02 (−0.03)
SER162	L1	0.11	0.03 (−0.08)	−0.07 (−0.18)	0.20 (0.09)
ASP163	L1	0.40	0.28 (−0.12)	0.39 (−0.01)	−0.27 (−0.67)
LYS165	L1	−0.50	−0.16 (0.34)	−0.26 (0.24)	0.46 (0.96)
PHE167	L1	−2.26	−3.14 (−0.88)	−1.59 (0.67)	**−4.87 (−2.61)**
ASN169	L1	−2.66	**0.00 (2.66)**	**0.09 (2.75)**	**−0.22 (2.44)**
TYR184	–	−2.41	−2.06 (0.35)	−1.44 (0.97)	−1.79 (0.62)
LEU185	L2	−0.07	−1.24 (−1.17)	−1.13 (−1.06)	−2.06 (−1.99)
LYS188	L2	−0.14	−0.07 (0.07)	−0.30 (−0.16)	0.02 (0.16)
ASP190	L2	0.26	−0.37 (−0.63)	0.20 (−0.06)	−0.10 (−0.36)
SER191	–	−0.03	0.00 (0.03)	0.00 (0.03)	0.01 (0.04)
GLY226	L3	−0.18	−0.57 (−0.39)	−0.07 (0.11)	−1.29 (−1.11)
THR227	L3	−0.30	−0.32 (−0.02)	−1.85 (−1.55)	**−2.90 (−2.6)**
HIS228	L3	−3.93	**0.14 (4.07)**	**−0.42 (3.51)**	**−1.12 (2.81)**
LEU229	L3	−4.53	**−0.70 (3.83)**	**−1.15 (3.38)**	**−2.07 (2.46)**
GLN231	L3	−0.52	**−2.75 (−2.23)**	−1.20 (−0.68)	0.14 (0.66)

Relative energy to p17.1 is in parenthesis. The amino acids may significant contribution with an absolute relative energy higher than 2 Kcal/mol are indicated in bold letters.

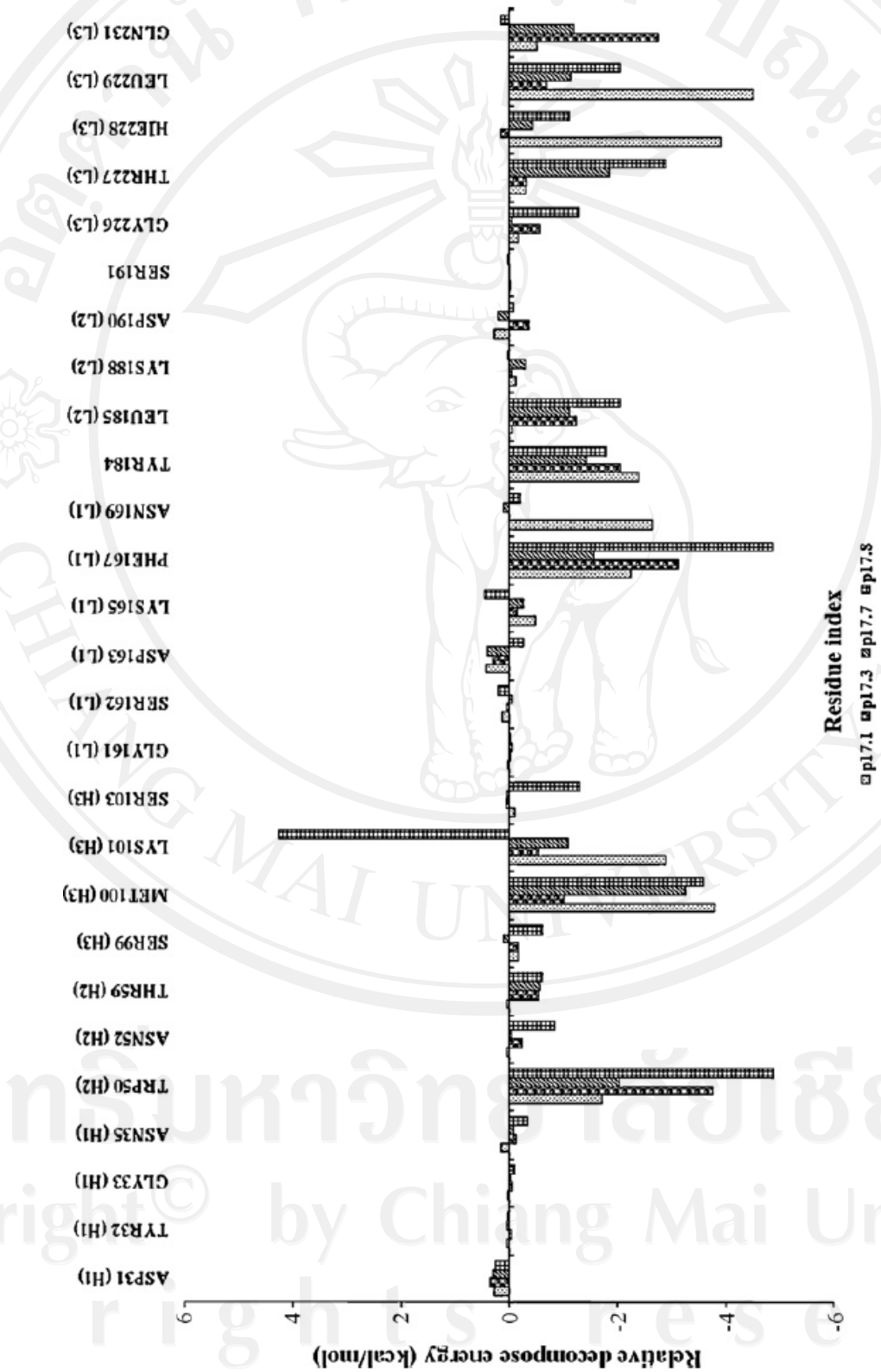

Figure 3.6A List of the decomposed energies of the common amino acids in CDRs of scFv-MA HB-8975.

The relative decomposed energy of each amino acid residue in CDRs with HIV-1 MA peptide epitopes is presented.

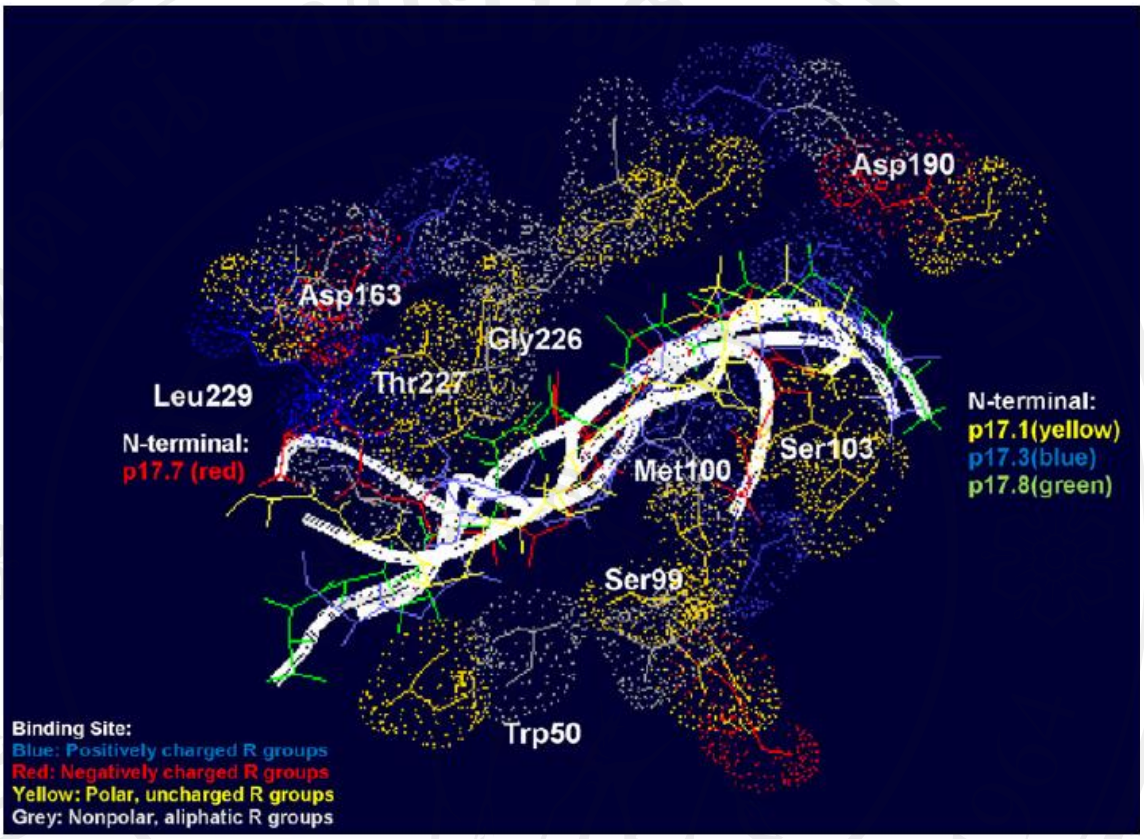

Figure 3.6B Residues interaction of final MD complex structure between scFv-MA HB-8975 and four peptide epitopes. The residues of scFv-MA HB-8975 binding strongly with the four peptides are indicated. The orientation of each peptide is shown.

3.8 Verification of computational data by site-specific mutagenesis

To verify whether the predicted data from computational approaches were trustworthy, site-specific mutagenesis was performed at amino acid residue Met100(H3) in scFv-MA HB-8975, since this residue exhibited a strong interaction with the wild type peptide p17.1 and the mutant peptides. Met100 was mutated to Gly100 (M100G) and Glu100 (M100E), resulting in pCom3X-scFv-MA M100G and pComb3X-scFv-MA M100E phagemid vectors. Phage-displayed scFv-MA mutants and soluble scFv-MA mutant were then produced and their binding activity was investigated by ELISA in comparison with scFv-MA HB-8975. As shown in **Figure 3.7**, the phage-displayed scFv-MA M100G showed a high signal that was comparable with the signal from phage-displayed scFv-MA HB-8975. However, the soluble scFv-MA M100G did not produce any signal. By contrast, both phage-displayed scFv-MA M100E and soluble scFv-MA M100E protein were negative for the p17.1 binding. These data suggested that scFv-MA M100G was active in the scFv-gpIII fusion protein on the phage particle but not in the soluble form, whereas no binding activity was found for scFv-MA M100E in either form. These results suggested that one amino acid mutation at Met100 to Gly100 abolished the binding activity of scFv-MA HB-8975 in the form of soluble protein, while mutation to Glu100 abolished the reactivity of both forms, scFv-gpIII fusion protein on phage particle and the soluble protein.

Competitive ELISA was employed to evaluate the binding affinity of phage-displayed scFv-MA M100G compared to scFv-MA HB-8975. Although the percentage of inhibition (PI) of scFv-MA M100G with four peptides represented the

same trend as shown by scFv-MA HB-8975, but the PI value was dramatically lower. Consequently, this result suggested that the binding affinity of scFv-MA HB-8975 with soluble peptides was reduced when amino acid residue Met100 was mutated to Gly100 **(Table 3.4).**

Taken together, the relevant information derived from computational analysis was reliable since it perfectly correlated with the data from the laboratory. This strategy was able to identify the specific residues in the scFv-MA HB-8975 that play a crucial role in the effective binding interaction with peptides. Based on this strategy, it will be applied to enhance the binding activity of scFv against its antigen by performing single-, double-, or multi-site directed mutagenesis.

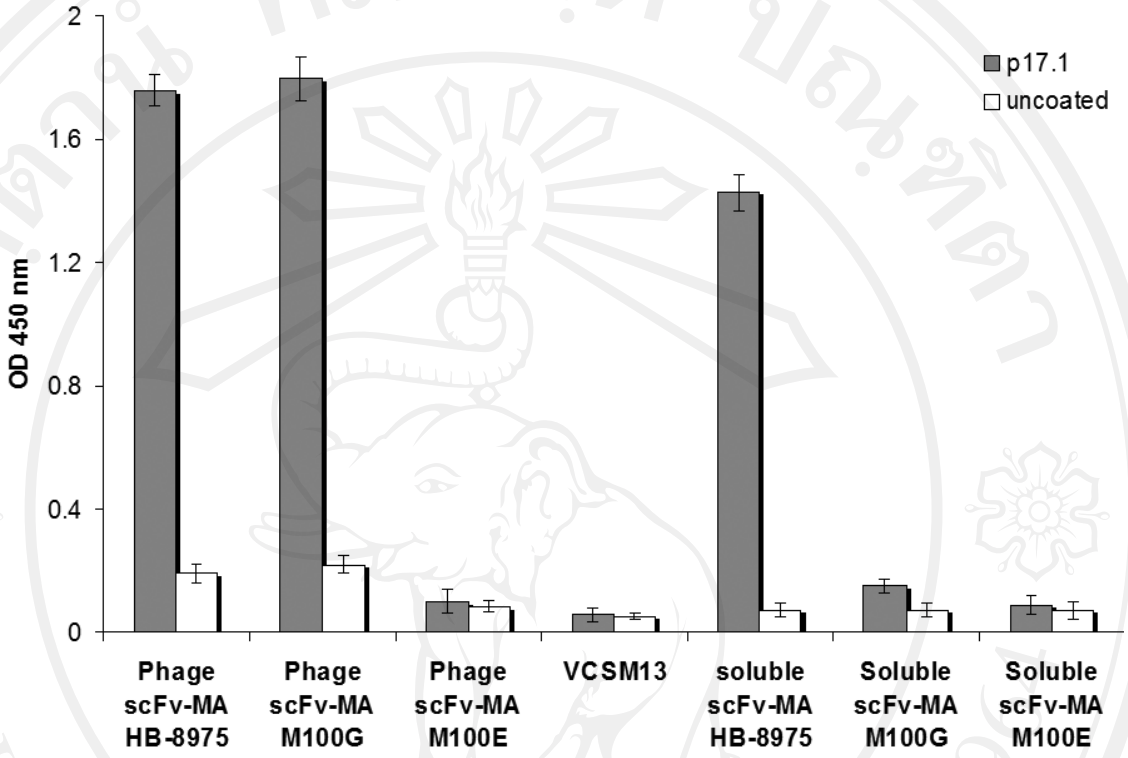

Figure 3.7 Characterization of scFv-MA mutants. Phage particles at 10^9 cfu/ml and 200 ug/ml of soluble protein were added into p17.1 peptide coated wells and traced by HRP-conjugated anti-M13 mAb and HRP-conjugated anti-HA tag mAb, respectively. VCSM13 was used as negative helper phage control.

Table 3.4 Comparison of the binding affinity of scFv-MA HB-8975 and scFv-MA M100G by percentage inhibition value.

Peptide names	Phage-displayed scFv-MA HB-8975	Phage-displayed scFv-MA M100G
p17.1	62.17	26.31
p17.3	45.66	13.42
p17.7	29.46	11.91
p17.8	67.10	36.04
CD147	5.54	2.56

Study 2: Generation of recombinant baculovirus-displayed scFv-MA HB-8975 by the novel leader sequence

3.9 Construction of scFv-MA HB-8975 in baculovirus expression system.

The rationale for the N-terminal modification was that the dipeptide Met-Gly at the N-terminus of scFvG2/MA represented a N-myristoylation signal which would promote the addressing scFvG2/MA to the same compartment as the N-myristoylated MA protein and Pr55Gag polyprotein (Carrière et al., 1995; Hong and Boulanger, 1993; Royer et al., 1991; Wilk et al., 2001). The gene encoding scFv-MA HB-8975 was cloned into pBluebac4.5 vector, namely pBlubac-scFv-MA vector. Afterward, two scFv-MA subclones, scFvE2/MA and scFvG2/MA, were generated by inserting particular oligonucleotides at the N-termius of scFv-MA in pBlubac4.5-scFv-MA vector. The ^{1}MEASLAAQAAQIQLVQSG^{18} was the N-terminal octadecapeptide sequence in scFvE2/MA, and ^{1}MGLAAQA- AQIQLVQSGPE^{18} was in scFvG2/MA. Both subclones were also modified at the C-terminus by the addition of a HA tag, the Influenza A virus hemagglutinin epitope YPYDVPDYA **(Figure 3.8).**

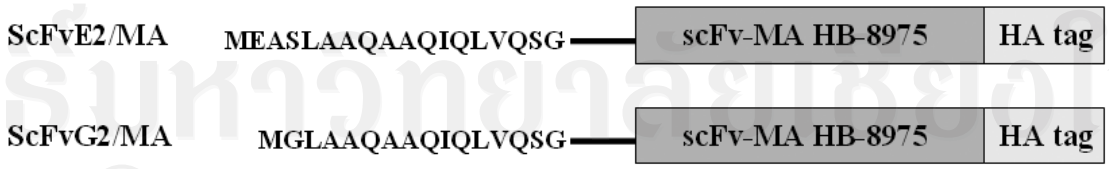

Figure 3.8 Amino acid sequences of scFvE2/MA and scFvG2/MA. The N-terminal octadecapeptide sequences were presented. Both scFvs contain HA tag at the C-terminus.

3.10 Production of baculovirus carrying scFv gene and expression of recombinant scFv in BV-infected Sf9 cells

Recombinant baculovirus expressing- scFvE2/MA (BV-scFvE2/MA) or –scFvG2/MA (BV-scFvG2/MA) were generated by performing cotransfection into Sf9 cells with pBluebac-scFvE2/MA or pBluebac-scFvG2/MA and linearized BV DNA. Subsequently, the recombinant baculovirus were isolated using blue plaque selection. Accordingly, BV-scFvE2/MA and BV-scFvG2/MA were obtained for further experiments.

To observe the kinetic expression of scFvs, Sf9 cells infected with BV-scFvE2/MA and scFvG2/MA were harvested at 24, 48, and 72 hr post infection (pi). The cells were lysed and the synthesis of scFvs in whole cell lysate was analyzed by Western blotting using anti-HA tag mAb. The extracellular culture medium was analyzed in parallel. As shown in **Figure 3.9**, the scFvE2/MA protein was detectable at molecular weight of 30 kDa as early as 24 hr, and was maximal at 72 hr pi. In contrast, scFvG2/MA was detected at later times (48 hr pi), and in 4- to 5-fold lower amounts, compared to scFvE2/MA at 48-72 hr pi **(Figure 3.9A)**. However, scFvE2/MA and scFvG2/MA proteins were stable over a period of 72 hr, with no major breakdown products detected in the Western blot patterns.

Moreover, cell lysates were then clarified by centrifugation, and scFvG2/MA and scFvE2/MA were probed in soluble fraction (S) and insoluble pellet (P), respectively. We found that 15-20% of the whole recombinant scFvE2/MA protein synthesized was recovered as soluble material, as determined by scanning and densitometric analysis of the protein bands on blots, with a maximum at 48 hr pi

(Figure 3.9B; leftmost half of the panel). The proportion of soluble scFvG2/MA was lower **(Figure 3.9B**; **rightmost half)**, with only 8-10% of scFvG2/MA protein recovered in the soluble fraction. The difference in the intracellular levels of the two recombinant proteins could not be explained by a higher level of scFvG2/MA secretion, compared to scFvE2/MA, as no scFvG2/MA protein was detected in the culture medium at any time pi. Only scFvE2/MA protein was detectable in the extracellular medium.

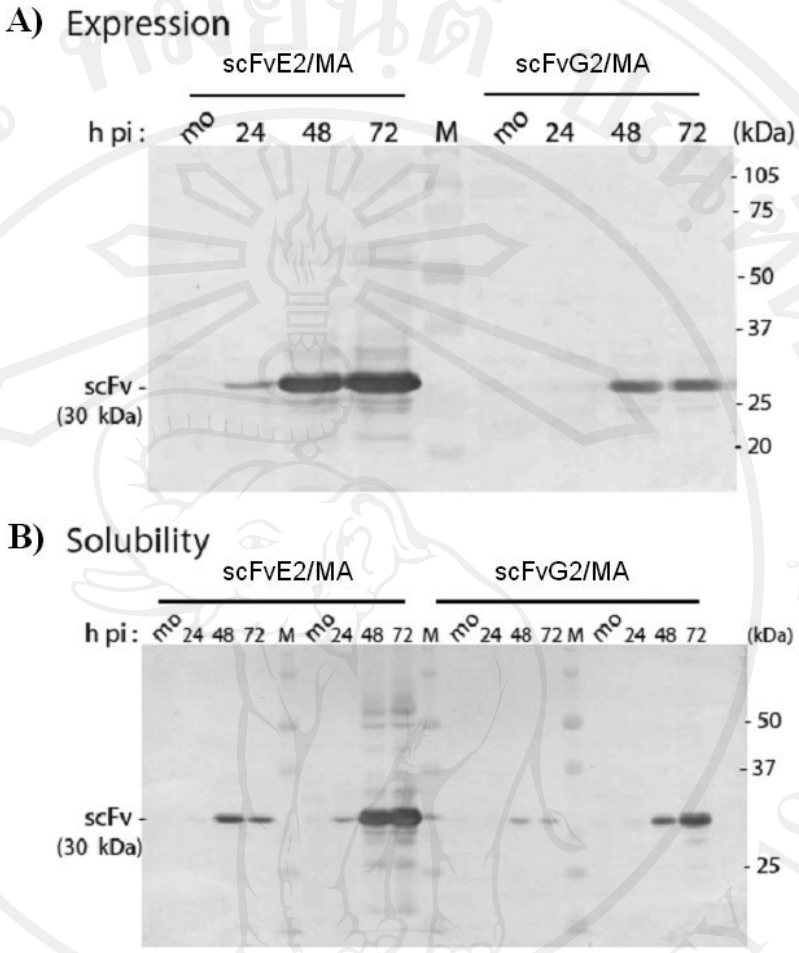

Figure 3.9 Expression and solubility of scFvE2/MA and scFvG2/MA in Sf9 cells. (A) Level of expression. Sf9 cells werbmock-infected (lanes mo), or infected with BV-scFvE2/MA or BV-scFvG2/MA, and harvested at 24, 48 and 72 hr pi, as indicated on top of the panel. Whole cell lysates were analyzed by SDS-PAGE and Western blotting using anti HA tag mAb. **(B)** Solubility. Lysates of mock-infected cells (mo) or BV-scFvE2/MA or BV-scFVG2/MA-infected cells harvested at 24, 48 and 72 hr pi, as indicated on top of the panel were clarified by centrifugation and soluble fraction (S) and pelletable material (P) analyzed as above. M, molecular mass markers, with their apparent molecular masses are indicated in kilodaltons (kDa) on the right side of the blots.

3.11 Cellular distribution of scFvE2/MA and scFvG2/MA in recombinant BV-infected Sf9 cells

To determine the subcellular localization of scFvE2/MA and scFvG2/MA proteins, cell fractionation was performed. The distinction between cytosol (Cy), membranes and organelles (Mb), nucleus (Nu) and cytoskeleton (Sk) was only operational, and did not preclude probable cross contaminations between different fractions. With this restriction in mind, scFvE2/MA was found to be associated with the cytosolic fraction and nuclear pellet in similar amounts (ca. 20-25% each), but larger quantities (50-60%) were recovered in the insoluble fraction of cytoskeletal proteins **(Figure 3.10A; leftmost half of the panel)**. Only small amounts of scFvE2/MA were detected in the membrane fraction **(Figure 3.10A**, **Mb lane)**. The pattern of subcellular localization was different for the scFvG2/MA protein, which was undetectable in the cytosolic and nuclear fractions, but distributed unequally between membrane and cytoskeletal fractions, two-thirds and one-third of the total, respectively **(Figure 3.10A**, **rightmost half of the panel)**. Thus, the N-terminal G2 mutation conferred two new properties to scFvG2/MA, compared to its scFvG2/MA counterpart, (i) a lower level of expression, and (ii) a relocation to and strong association with the membranal fraction. The membrane association of scFvG2/MA determined by cell fractionation was a prior consistent with the membrane targeting expected for a N-myristoylated protein.

In addition, cellular localization of scFvE2/MA and scFvG2/MA was further studied *in situ*. BV-infected Sf9 cells were harvested at 48 hr pi and examined in flow cytometry using anti-HA tag mAb. The HA tag-positive cells confirmed the

accessibility of scFvE2/MA at the surface of infected Sf9 cells, and the absence of significant amounts of scFvG2/MA molecules at the cell surface **(Figure 3.10B).** Considering, the poor recovery of scFvE2/MA in the membranal fraction upon cell fractionation (refer to **Figure 3.10A**), the results of flow cytometry suggested that the majority of scFvE2/MA molecules were addressed to the plasma membrane and highly accessible at the cell surface, but proned to dissociate from the membrane upon cell disruption and fractionation, and to relocate into the soluble fraction. In contrast, we observed a major intracellular retention of most of the scFvG2/MA molecules. Together with the data of cell fractionation **(Figure 3.10A)**, this suggested that scFvG2/MA protein was in majority sequestered in the intracellular membrane network.

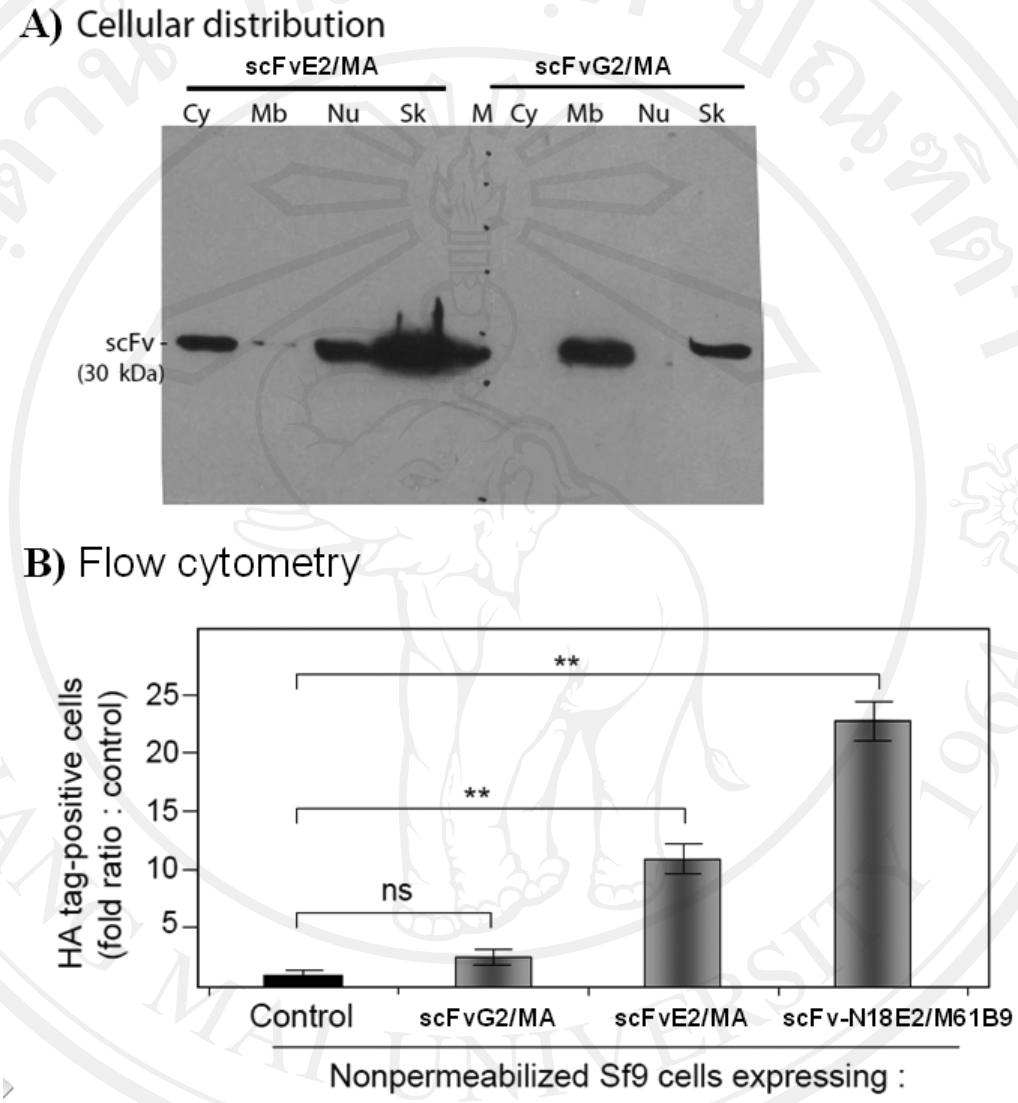

Figure 3.10 Cellular localization of scFvE2/MA and scFvG2/MA in Sf9 cells. (A) Cell fractionation. Sf9 cells infected with BV-scFvE2/MA or BV-scFvG2/MA as indicated on top of the panel were harvested at 48 hr pi and processed for cell fractionation into cytosolic compartment (Cy), membranes (Mb), nuclear compartment (Nu) and cytoskeletal-associated proteins (Sk). Subcellular fractions were analyzed by SDS-PAGE and Western blotting using anti-HA tag antibody. **(B)** Flow cytometry. Nonpermeabilized Sf9 cells expressing scFvE2/MA, scFvG2/MA or the scFv-N18E2/M6 chimera were harvested at 48 hr pi, reacted with anti-HA tag mAb and analyzed by flow cytometry. Results shown were the proportion of HA tag-positive cells, expressed as the fold ratio over the values of control cells, attributed the value of 1. Control consisted of BVCAR-infected cells, i.e. cells expressing irrelevant membrane glycoprotein. BVCAR was a recombinant BV expressing the human CAR glycoprotein, and BVCAR-infected cells released CAR displaying virions in the extracellular medium (Granio et al., 2009). Average of three separate experiments, m ± SEM; (**), $P < 0.01$; ns, not significant.

3.12 Characterization of purified scFvE2/MA and scFvG2/MA

To test the binding activity of scFvE2/MA and scFvG2/MA, soluble scFvs were purified from clarified lysates of cells expressing scFvMA by adsorption onto anti-HA tag-agarose gel and specific elution of the scFv-MA proteins was carried out using HA peptide containing buffer. Subsequently, the purified scFvs were added into p17.1 peptide epitope coated well and followed by anti-HA tag mAb. As shown **in Figure 3.11A**, the binding data from indirect ELISA clearly showed that recombinant scFvE2/MA and scFvG2/MA reacted with its specific peptide epitope indicating that the ability of two versions of scFv-MA had no different.

To assess the stringency of scFvE2/MA and scFvG2/MA towards HIV-1 MAp17 variants, five different p17 peptide epitoes were tested versus the original peptide epitope p17.1 in competition ELISA. All p17 peptide variants competed with p17.1 to significant levels, considering that control homologous competition (bound p17.1 *vs* free p17.1) showed a 90% binding inhibition of scFvE2/MA **(Figure 3.11B)**. The lowest competition was observed for peptide p17.7. Competition ELISA was also performed using p17.1 *versus* a synthetic peptide of identical composition but of inverted sequence, YNQSVQSSHGTD. No competition was observed **(Figure 3.11B)**, implying that N-to-C orientation of the peptide sequence and the C-terminal position of tyrosine residue-132 were crucial for the recognition of the epitope by scFvE2/MA. The affinity and binding specificity of scFvG2/MA to the different p17 peptide epitopes was also tested using competition ELISA. No significant difference was observed between scFvG2/MA and scFvE2/E2 in terms of reactivity with HIV-1 MA epitope variants **(Figure 3.11B)**. The lack of difference in the antigen binding

function of soluble scFvG2/MA and scFvE2/MA indicated that the apparent poorer solubility of scFvG2/MA compared to scFvE2/MA was likely due to its addressing to membranal and cytoskeletal compartments and not to major changes in its overall conformational structure and/or complementary-determining regions. This underlined the importance of the N-terminal sequence, which harboured the only difference between scFvG2/MA and scFvE2/MA. Regarding the address and solubility, scFvE2/MA was further analyzed the accessible property on the baculovirus cell surface.

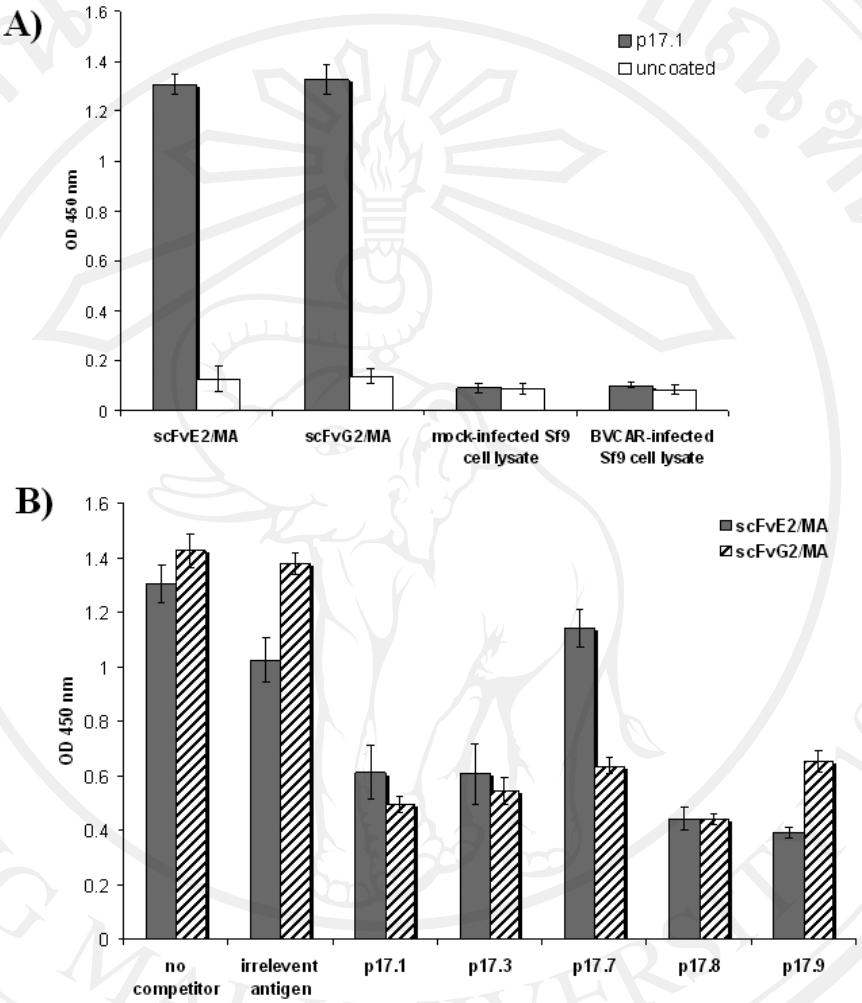

Figure 3.11 Immunological Characterization of scFvE2/MA and scFvG2/MA. (A) Indirect ELISA with p17.1 peptide. The purified scFvE2/MA and scFvG2/MA were analyzed using p17.1 coated wells. Negative control consisted of mock-infected Sf9 cell lysate and BVCAR-infected cell lysate (irrelevant recombinant protein). **(B)** Competitive ELISA with p17 peptide variants. The affinity of soluble scFvs was tested using solid adsorbed p17 versus soluble p17.1 or p17 peptide epitopes p17.3, p17.7, p17.8, and p17.9. ELISA performed in the absence of competitor and in the presence of irrelevant antigen was used as negative controls.

3.13 Biophysical status of scFvE2/MA on the baculovirus

As mentioned, a significant amount of scFvE2/MA protein was recovered in the extracellular medium of BV-scFvE2/MA-infected Sf9 cells. These extracellular scFvE2/MA molecules might occur as soluble protein, or as particle associated material, e.g. released within membrane microvesicles or exosomes, or associated with cell debris. In order to determine the status of extracellular scFvE2/MA protein, samples from culture mediun were subjected to isopycnic ultracentrifugation analysis in sucrose-D2O density gradients (DaFonseca S, 2007; Hou et al., 2008). Gradient fractions were analyzed by SDS-PAGE and Western blotting, using anti-baculoviral envelope glycoprotein GP64 and anti-HA tag mAb. The fractions positive for the C-terminal HA tag of scFvE2/MA coincided with the anti-GP64-reacting fractions, and corresponded to particulate material sedimenting with the apparent density of BV particles of the viral progeny, d = 1.15-1.08 **(Figure 3.12)**. This suggested that scFvE2/MA was associated with the BV particles, either coencapsidated with the baculoviral proteins or inserted into the viral envelope. In the latter case, scFvE2/MA molecules could be exposed at the surface of the BV particles with their active site accessible for epitope binding.

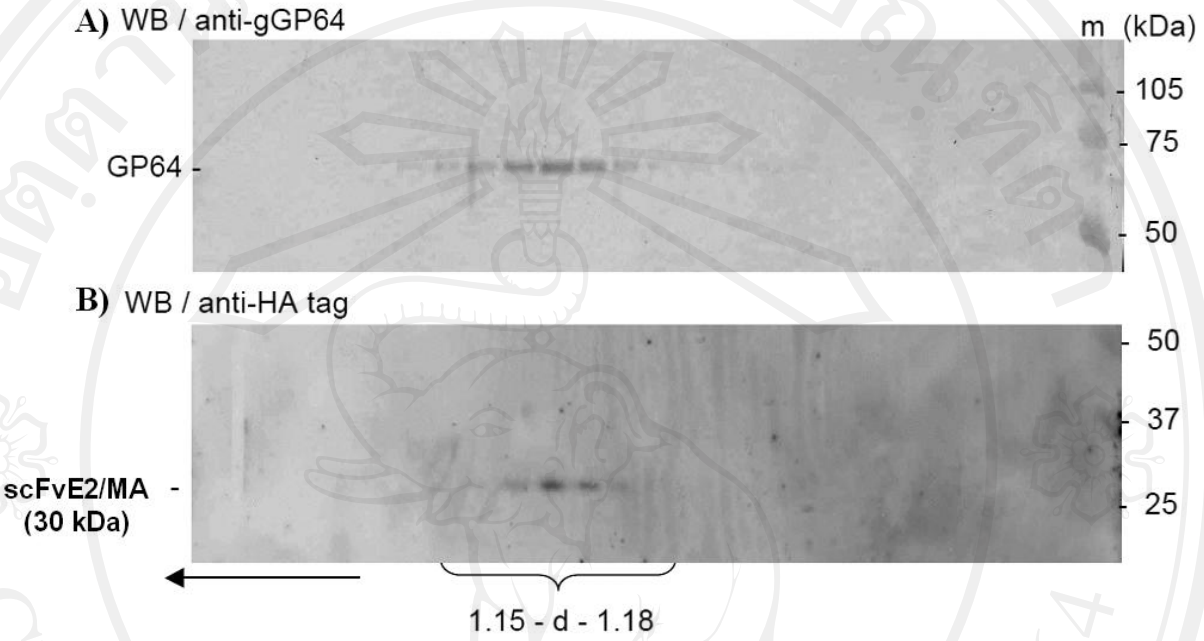

Figure 3.12 BV display of scFvE2/MA (BV-E2/MA). Samples of culture medium of Sf9 cells infected with BV-scFvE2/p17 were harvested at 72 hr pi and analyzed by isopycnic ultracentrifugation in sucrose-D20 gradients, as described under Materials and Methods. Gradient fractions were analyzed by SDS-PAGE and Western blotting, using **(A)** monoclonal antibody to the baculoviral GP64 envelope glycoprotein for detection of baculovirus progeny, and (**B)** anti-HA tag mAb for detection of scFvE2/MA.

3.14 Immuno-EM analysis of baculoviral progeny of BV-scFvE2/MA

In order to confirm the reality of this surface exposure, samples of extracellular medium of BV-scFvG2/MA- and BV-scFvE2/MA-infected Sf9 cells were analyzed by isopycnic ultracentrifugation in sucrose-D2O gradients, and fractions sedimenting at 1.15-1.08 were deposited on grids, immunogold labeled with anti-HA tag mAb, and observed under the electron microscope. As shown in **Figure 3.13**, BV-scFvG2/MA virions were never seen associated with gold grains, and most immunogold labeling was found at distance from BV particles, and corresponded to nonspecific, background labeling (not shown). The absence of anti-HA tag labeling of BV-scFvG2/MA virions in immuno-EM was consistent with the absence of detectable scFvG2/MA protein in the extracellular medium, as mentioned above. Under the same experimental conditions however, anti- HA tag immunogold labeling was found to be associated with virions of BV-scFvE2/MA. The immuno-EM analysis therefore confirmed that scFvE2/MA molecules were truly incorporated into the baculoviral envelope. Such incorporation of foreign proteins into the baculoviral envelope has already been described with human membrane glycoprotein CAR (DaFonseca S, 2007).

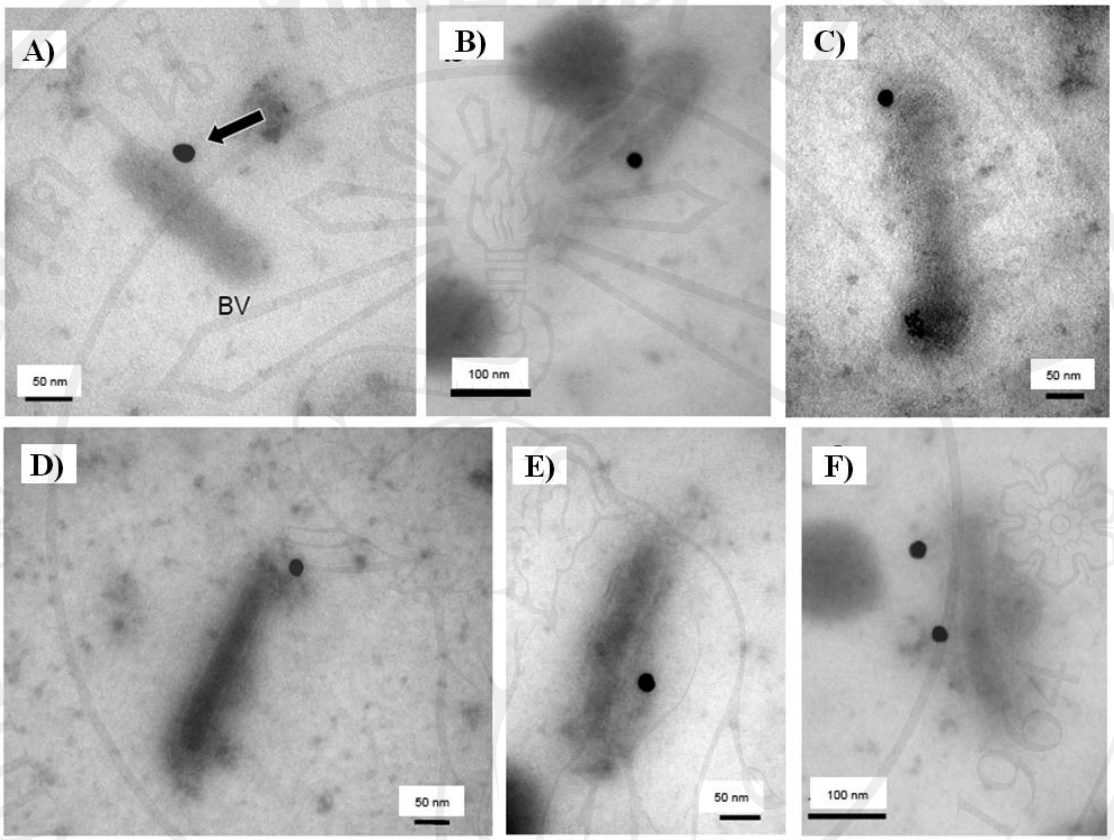

Figure 3.13 Immuno-electron microscopy of BV particles carrying scFvE2/MA (BV E2/MA). Samples of baculovirus progeny recovered from the culture medium of Sf9 cells infected with BV-scFvE2/MA and harvested at 72 hr pi were deposited on grids and negatively stained with uranyl acetate. Specimens were reacted with anti-HA tag mAb, followed by anti-mouse immunoglobulins antibody coupled to 20-nm colloidal gold grains. Different fields are presented in panels **(A)** to **(F)**. Arrow in (**A)** points to a gold grain associated with a BV particle (BV). In (**F)**, two gold grains are seen associated with one BV particle.

3.15 Immunological functionality and topology of scFvE2/MA displayed on baculoviral envelope

The observation that BV-displayed scFvE2/MA was accessible to anti-HA tag mAb in immuno-EM analysis strongly suggested that the C-terminal HA tag was oriented outwards. The next experiments were designed to assess the topological orientation of the scFvE2/MA molecule in the baculoviral envelope, and, more importantly, to determine the degree of accessibility of its antigen binding regions. BV-scFvE2/MA virions were immobilized on ELISA plate and probed with anti-HA tag mAb. The positive reaction indicated that the carboxyterminal region of scFvE2/MA was exposed at the surface of the virions **(Figure 3.14A)**, and that the insertion of scFvE2/MA in the baculoviral envelope mimicked the orientation of class II membrane glycoproteins, with the aminoterminal region anchored in the baculoviral envelope, as depicted in **Figure 3.14C.** The antigen binding activity of BV-displayed scFvE2/MA was then determined by ELISA, using immobilized synthetic peptide p17.1. In this assay, BV-scFvE2/MA virions displaying scFvE2/MA were used as the equivalent of primary antibodies, and bound virions were detected using monoclonal antibody directed towards the baculoviral glycoprotein GP64. The p17.1 peptide were recognized by BV-scFvE2/MA virions **(Figure 3.14B)**, which indicated that the BV-displayed scFvE2/MA molecules retained their antigen-binding capacity.

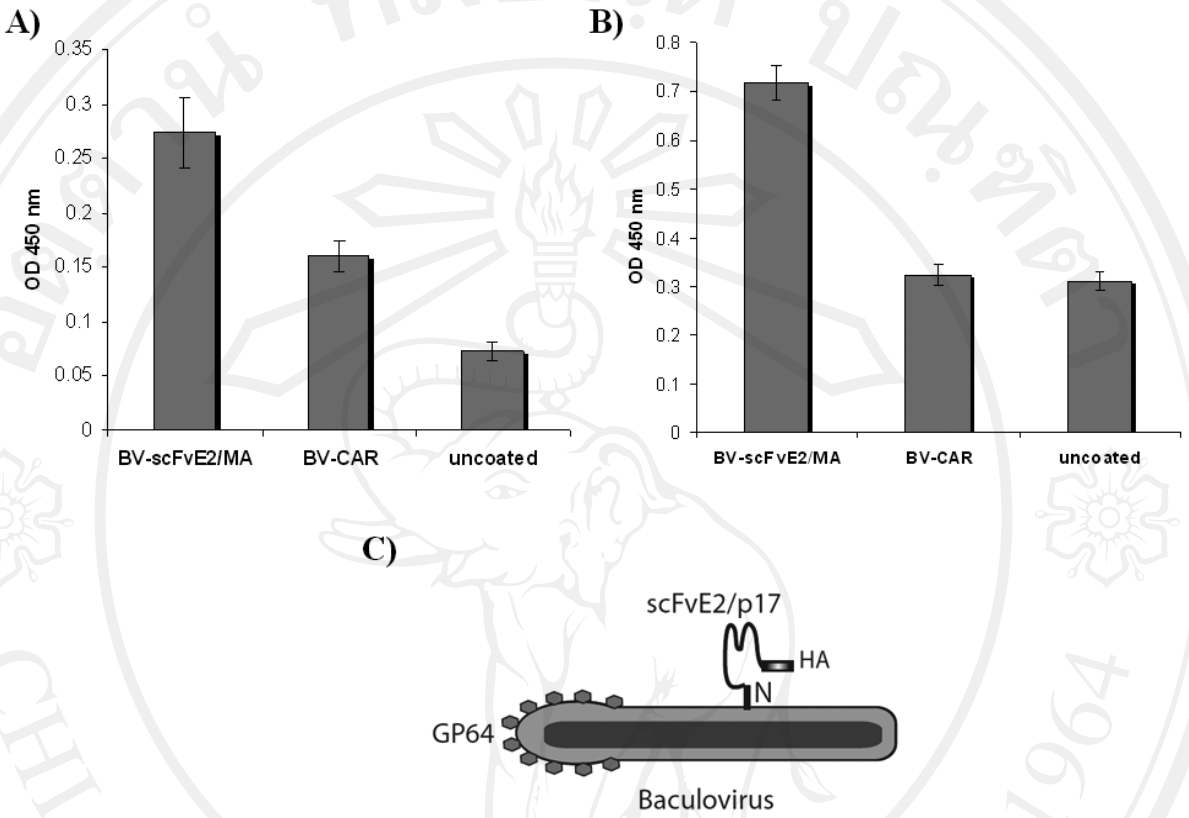

Figure 3.14 Topology and functionality of BV-displayed scFvE2/MA. Baculoviral progeny recovered from the culture medium of Sf9 cells infected with BV-scFvE2/MA was isolated by ultracentrifugation. **(A)** BV-scFvE2/MA virions were immobilized on ELISA plate and reacted with anti-HA tag mAb and peroxidase-labeled complementary antibody. Controls were uncoated well, and well coated with irrelevant baculovirus particles (CAR-displaying BVCAR; (DaFonseca S, 2007). **(B)** GP64, baculoviral envelope major glycoprotein. BV-scFvE2/ pMA virions were reacted in ELISA with immobilized synthetic p17.1 peptide. (**C)** Schematic model of scFvE2/MA molecule displayed at the surface of a BV particle. Average of three separate experiments, m ± SEM; (*), $P < 0.05$); (**), $P < 0.01$).

3.16 Baculovirus displayed scFv-M61B9 against CD147 molecules

3.16.1 Immu-electron microscopy

Although scFvE2/MA did not contain any consensus signal peptide for membrane addressing, we postulated that in Sf9 cells, the N-terminal octadecapeptide sequence ^{1}MEASLAAQAAQIQLVQSG^{18} (abbreviated N18E2), was responsible for the intracellular trafficking and targeting of scFvE2/MA to the site of BV budding, where it became inserted into the baculoviral envelope. To test this hypothesis, N18E2 was fused to the N-terminus of a non-related scFv, the HA-tagged scFv-M61B9, which recognizes the membrane glycoprotein CD147 (Intasai et al., 2009; Tragoolpua et al., 2008). The chimeric scFv construct, abbreviated scFv-N18E2/M61B9, was expressed in Sf9 cells using a recombinant BV vector (BV-N18E2/M61B9). ScFv-N18E2/M61B9 molecules were detected in significant levels at the surface of nonpermeabilized cells harvested at 48 hr pi, as for scFvE2/MA **(refer to Figure 3.10B)**. The baculoviral progeny from BV-N18E2/M61B9-infected cells was then isolated by ultracentrifugation and analyzed by ELISA (not shown) and immuno-EM **(Figure 3.15A)** using anti-HA tag mAb. Both methods showed the accessibility of the HA tag at the surface of BV particles. In the electron micrograph shown in **Figure 3.15A(D)**, two baculovirus particles were seen as a V-shape dimer pointing to one gold grain. This might represent the cross-linking of two particles via the two Fab domains of a single antibody molecule, although it could not be excluded that one antibody would bind to one particle, while the other would be in close proximity.

3.16.2 Indirect ELISA

The antigen-binding capability of BV-displayed chimeric scFv-N18E2/M61B9 was also tested using the recombinant CD147-BCCP fusion protein as immobilized antigen in ELISA, as previously described (Tragoolpua et al., 2008). The data showed that the chimeric scFv-N18E2/M61B9 molecules present at the surface of BV particles conserved their antigen-binding function and their specificity towards CD147 **(Figure 3.15B).** These results suggested that the fusion of the N18E2 peptide to scFv-M61B9 was able to confer to the chimeric scFv-N18E2/M61B9 protein the capacity to be addressed to the BV budding sites at the plasma membrane and to be incorporated into the baculoviral envelope. They also suggested that N18E2 could function as a universal N-terminal signal peptide for BV-display of functional scFv of biological interest.

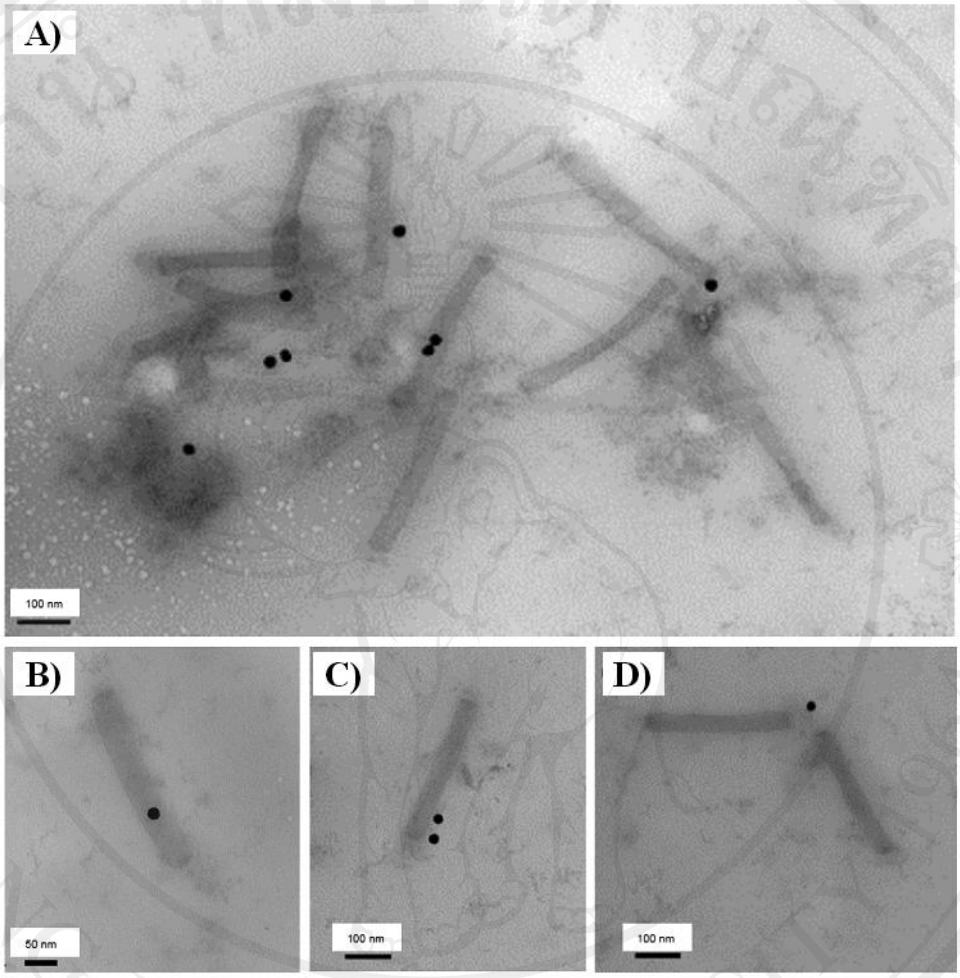

Figure 3.15A Immuno-electron microscopy of BV particles carrying chimeric scFv-N18E2/M6 (BV-N18E2/M61B9). Samples of baculoviral progeny recovered at 72 hr pi from the culture medium of Sf9 cells infected with BV-N18E2/M61b9 were deposited on grids and negatively stained with uranyl acetate. Specimens were reacted with anti-HA tag mAb, followed by anti-mouse immunoglobulins antibody coupled to 20-nm colloidal gold grains. Different fields are presented in panels **(A)** to **(D)**. **(A)**, General view of a cluster of immunogold-labeled BV-N18E2/M61B9 particles. **(B-D)**, Enlargement of immunogold-labeled BV-N18E2/M61B9 particles.

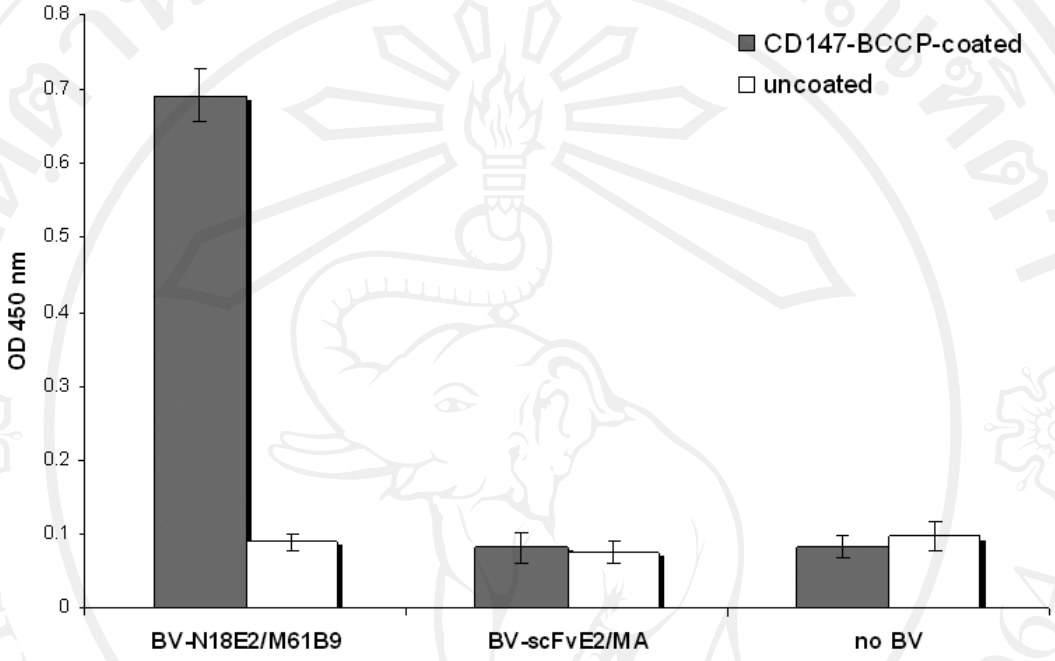

Figure 3.15B Functional analysis of BV-displayed chimeric scFv-N18E2/M61B9. The antigen-binding capacity and specificity of chimeric scFvE2/M61B9 displayed on the BV particle envelope was assessed by indirect ELISA, as described in a previous study [38,39]. Aliquots of BV-N18E2/M61B9 and control BV-scFvE2/MA particles recovered from BV infected Sf9 cells were added to CD147-BCCP-linked avidin-coated wells, and incubated for 1 hr at RT. After washing steps, bound viral particles were detected by addition of anti baculoviral envelope glycoprotein GP64 in TBS-BSA. Average of three separate experiments, m ± SEM. (**), $P < 0.01$.

3.17 A scheme of the general strategy of BV particle display using the novel leader octadecapeptide N18E2

The general strategy of stepwise construction of BV particles displaying scFv molecules of interest equipped with our signal octadecapeptide N18E2 is presented in **Figure 3.17.** The PCR amplification of the scFv coding sequence was performed using a Fw 5´-primer containing a *Nhe I* site and the N18E2 coding sequence and Rev 3´-primer encoding a HA tag and a *Hind III* site **(Figure 3.16(1))**. Afterward, the N18E2-scFv-HA-encoding DNA fragment was inserted into the baculoviral intermediate plasmid pBlueBac4.5, digested with *Nhe I* and *Hind III* **(Figure 3.16(2))**. The pBlueBac4.5-N18E2-scFv-HA and linearized baculoviral DNA were cotransfected into insect cells and homologous recombination was occurred **(Figure 3.16(3))**. The positive plaques were selected for recombinant baculoviral clone harboring N18E2-scFv-HA (e.g. blue plaque selection) and then amplification and isolation of recombinant BV expressing N18E2-scFv-HA were perform. Finally, the baculovirus displayed N18E2-scFv-HA was obtained **(Figure 3.16(4))**.

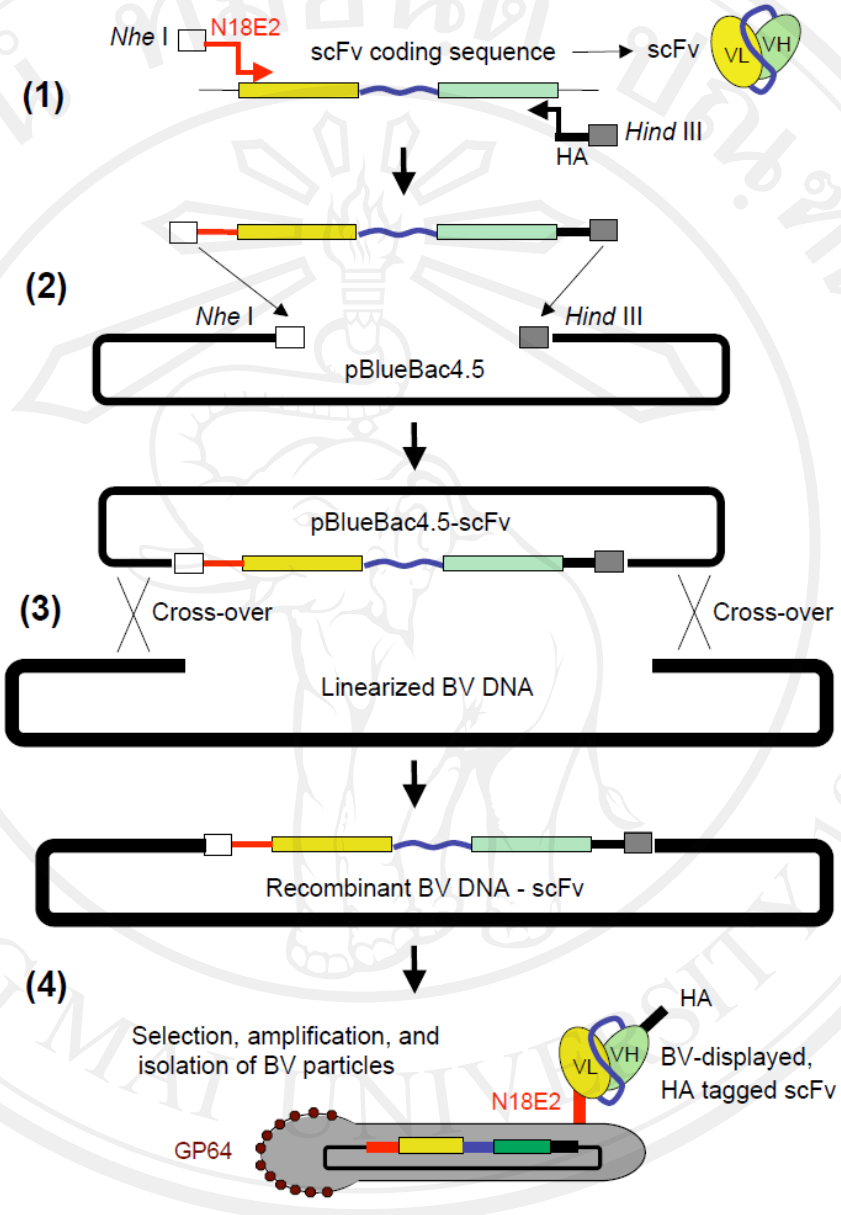

Figure 3.16 Generation of recombinant BV vector designed for the display of scFv using the N18E2 signal peptide. Shown is the stepwise construction and isolation of BV-N18E2/scFv, a recombinant BV designed to expose at its surface scFv molecules of interest equiped with the signal octadecapeptide N18E2.

Study 3: Development of a simplified enzyme-linked immunosorbent assay (ELISA) for the HIV-1 protease (HIV-PR) activity.

3.18 Design of the ELIS-based HIV-PR activity assay (ELIB-PA)

We have generated a novel, immunological *in vitro* assay to determine the proteolytic activity of HIV-PRH_6, designated the "ELIS-based HIV-PR activity assay" or "ELIB-PA". As shown in **Figure 3.17**, a microplate well was pre-coated with nickel to capture the substrate (H_6MA-CA) via an N-terminal His_6 tag. As a result, the MA domain was contiguous to the polystyrene surface, whereas the CA domain was protruding outwards and more accessible **(Figure 3.17A).** The protease substrate H_6MA-CA was cleaved upon addition of a bacterial extract containing the soluble enzyme HIV-PRH_6, resulting in the release of the CA domain and the unmasking of the carboxylterminal epitrope of the MA domain **(Figure 3.17B–C).** With this method, the proteolytic activity of HIV-PRH_6 was detected using the special characteristics of two monoclonal antibodies, anti-CA mAb G18 and anti-cleaved MA mAb HB-8975 **(Figure 3.17D).** The decreased detection of CA and the increased detection of the C terminus of MA are indicative of HIV-PRH_6 activity. This assay provides a high-throughput platform for both validating the efficiency of newly developed drugs *in vitro* and facilitating the discovery of new PIs. In addition, it can serve as a tool for examining the influence of various mutations in HIV-PRs isolated from drug-resistant strains.

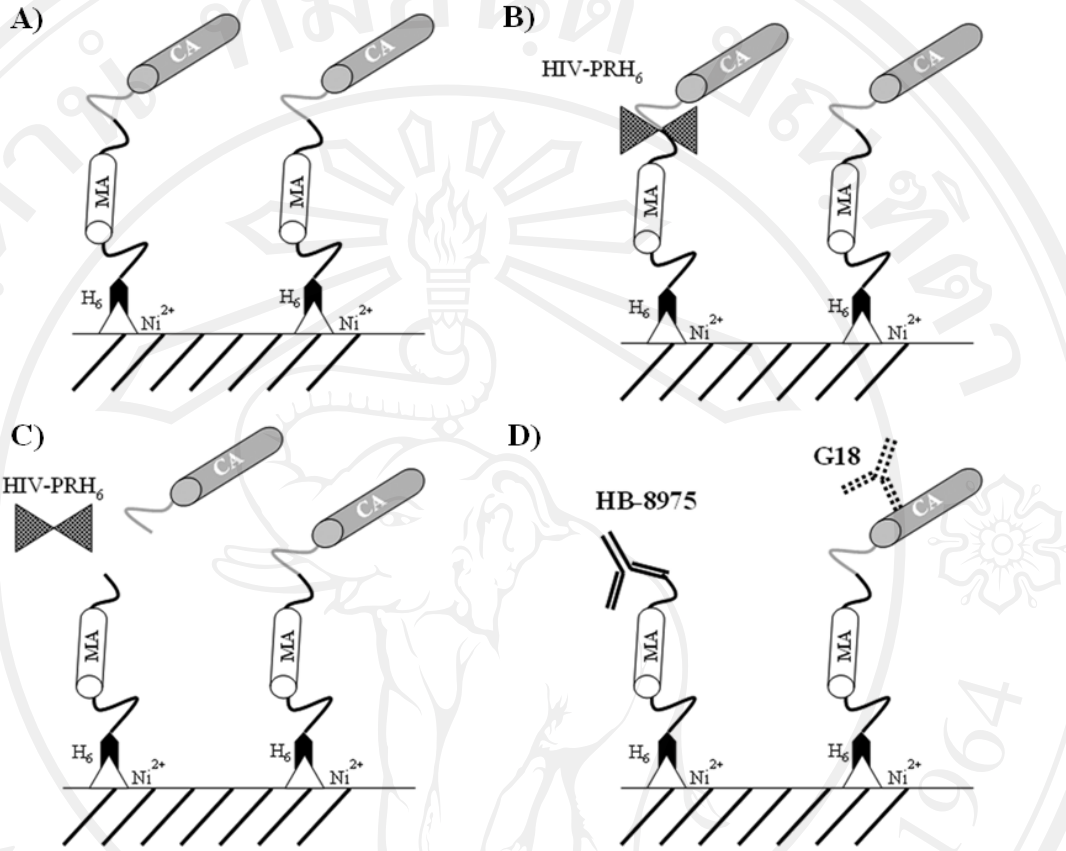

Figure 3.17 Principle of the *in vitro* ELIS-based HIV-PR activity assay. **(A)** First, H_6MA-CA is immobilized on the surface of the well via the interaction between the N-terminal His_6 tag and plate-bound Ni^{2+}. **(B)** Next, HIV-PRH_6 is added, and it recognizes the peptide epitope of the MA next to the cleavage site between the MA and CA domains. **(C)** Following proteolytic cleavage of the substrate, the CA domain is released from the H_6MA. (**D)** The proteolytic activity of HIV-PRH_6 can be detected by the change in the binding of two antibodies (anti-CA mAb G18 and anti-MA mAb HB-8975) that recognize specific regions; anti-MA mAb HB-8975 recognizes the newly exposed free C- terminal region of MA, whereas anti-CA mAb G18 binds to the CA domain.

3.19 Construction of a plasmid vector encoding HIV-PRH_6

The gene encoding HIV-PRH_6 was amplified and cloned into pET21a, resulting in the pET21-HIV-PRH_6 construct shown in **Figure 3.18A**. Expression in this system is controlled via the strong bacteriophage T7 transcription/translation signals and *lacUV5* regulatory elements. HIV-PR is composed of 99 amino acids, which are underlined in **Figure 3.18B.** An additional 12 amino acids were added in our construct: 4 amino acids from the added restriction site at the N terminus, 2 amino acids (GA) as a small linker and a C-terminal His_6 tag for detection purposes. Therefore, the resulting recombinant HIV-PRH_6 is 111 amino acids long. In this study, we also constructed an HIV-PR variant, HIV-PRH_6 I54V that has an amino acid substitution at position 54 (isoleucine to valine), to evaluate the HIV-PR activity assay.

A)

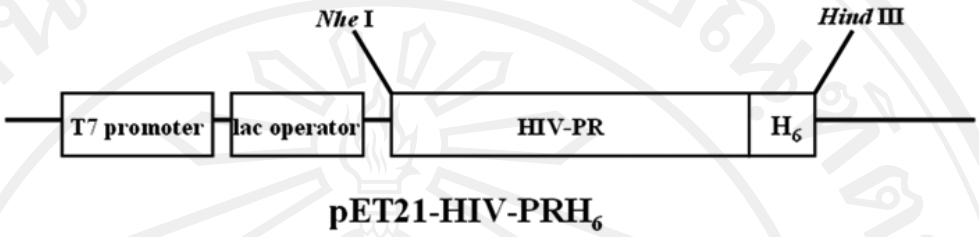

B)

```
                    10        20        30        40
                    ....|....|....|....|....|....|....|....|
HIV-PRH6            MASMPQITLWKRPLVTIKIGGQLKEALLDTGADDTVLEEM 40
HIV-PRH6 I54V       ........................................ 40

                    50        60        70        80
                    ....|....|....|....|....|....|....|....|
HIV-PRH6            NLPGRWKPKMIGGIGGFIKVRQYDQIIIEICGHKAIGTVL 80
HIV-PRH6 I54V       ................V....................... 80

                    90        100       110
                    ....|....|....|....|....|....|..
HIV-PRH6            VGPTPVNIIGRNLLTQIGCTLNFGAHHHHHH* 112
HIV-PRH6 I54V       ..............................* 112
```

Figure 3.18 Construction of an HIV-PRH$_6$ expression vector and the amino acid sequence of HIV-PRH$_6$ and its variant. (A) The gene encoding HIV-PR containing a His$_6$ tag at the C terminus was inserted into pET21a, resulting in pET21-HIV-PRH$_6$. **(B)** HIV-PRH$_6$ is 111 amino acid-long and includes the 99 amino acids of HIV-PRH$_6$ (underlined), 4 amino acids resulting from the addition of a restriction site at the N-terminus, a short, 2–amino acid linker, and the 6 amino acids of the His$_6$ tag at the C-terminus. The variant, HIV-PRH$_6$ I54V, contains an amino acid substitution at position 54 (I → V).

3.20 Production and solubility of HIV-PRH_6 in E. coli

Since the overexpression of HIV-PR may be toxic to the cell, we optimized the induction temperatures to be 16°C and 30°C to prevent the cell death. Furthermore, a low concentration of IPTG was used for induction. The HIV-PRH_6 migrated at an apparent molecular weight of approximately 12 kDa. Comparison of the soluble fraction of HIV-PRH_6 obtained at different induction temperatures showed that the solubility at 16°C was superior to that at 30°C **(Fig. 3.19A),** indicating that the production and solubility of HIV-PRH_6 was deeply affected by the temperature. The level of protein expression was also compared between wild-type HIV-PRH_6 and HIV-PRH_6 I54V mutant, as estimated from the intensity of protein bands in SDS-PAGE and Western blot analysis. As shown in **Figure 3.19B**, the amount of HIV-PRH_6 was lower than that of HIV-PRH_6 I54V, for the same amount of total protein loaded. The expression ratio of HIV-PRH_6 to HIV-PRH_6 I54V was found to be 1: 1.5. This result suggested that the amino acid substitution at position 54 had slightly affected on the increment of protein production or solubility.

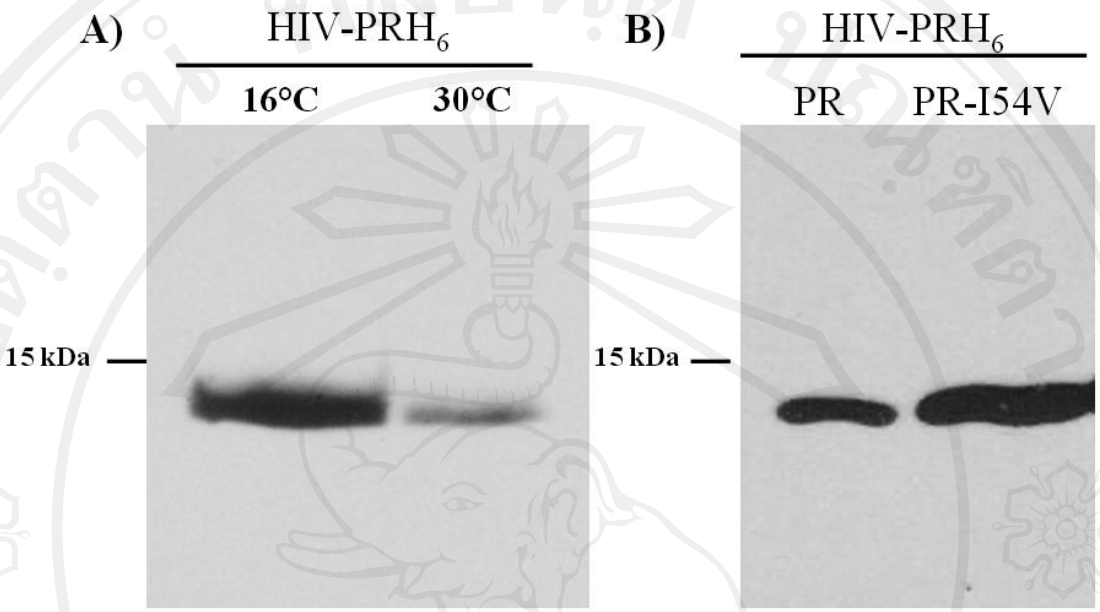

Figure 3.19 Expression of HIV-PRH$_6$ and its variant in *E. coli.* Western blot analysis of soluble HIV-PRH$_6$ and HIV-PRH$_6$ I54V from *E. coli* strain BL21(DE3) using an anti-His6 antibody. The size of the recombinant proteins is indicated. **(A)** The induction temperature was optimized at 16°C and 30°C. (**B)** A comparison of the expression level and solubility of HIV-PRH$_6$ and HIV-PRH$_6$ I54V under the same induction conditions.

3.21 Production and purification of recombinant H_6MA-CA protein in Sf9 cells

The DNA fragment coding for MA-CA, a non-N-myristoylated, carboxyterminal-truncated version of HIV-1 Gag polyprotein containing the matrix (MA) and capsid (CA) domain, was cloned into *Nhe* I and *Kpn* I site of pBlueBac4.5-His resulting in pBlueBac4.5-H_6MACA. This constructed transfer plasmid was cotransfected with linearized BV DNA into Sf 9 cells. The recombinant BV, abbreviated BV-H_6MA CA, from transfected cells was isolated using blue plaque selection. The infected cells harboring recombinant BVs showed the blue plaque appearance after beta-galactosidase staining were picked and used for protein production. A large amount of recombinant H_6MA-CA protein was produced in Sf9 cells infected with BV-H_6MA-CA. Infected cells were harvested at 48 hr post infection (pi), and recombinant H_6MA-CA were recovered from clarified cell lysate by Ni2+-NTA agarose column. The reactive bands coresponding to the molecular mass of H_6MA-CA protein were detected at approximately 40 kDa. The recombinant protein could be isolated with high purity as shown in **Figure 3.20**. This purified protein was dialyzed against PBS and ready for being a substrate for HIV-PRH_6 detected by anti-CA mAb G18 and anti-MA mAb HB-8975.

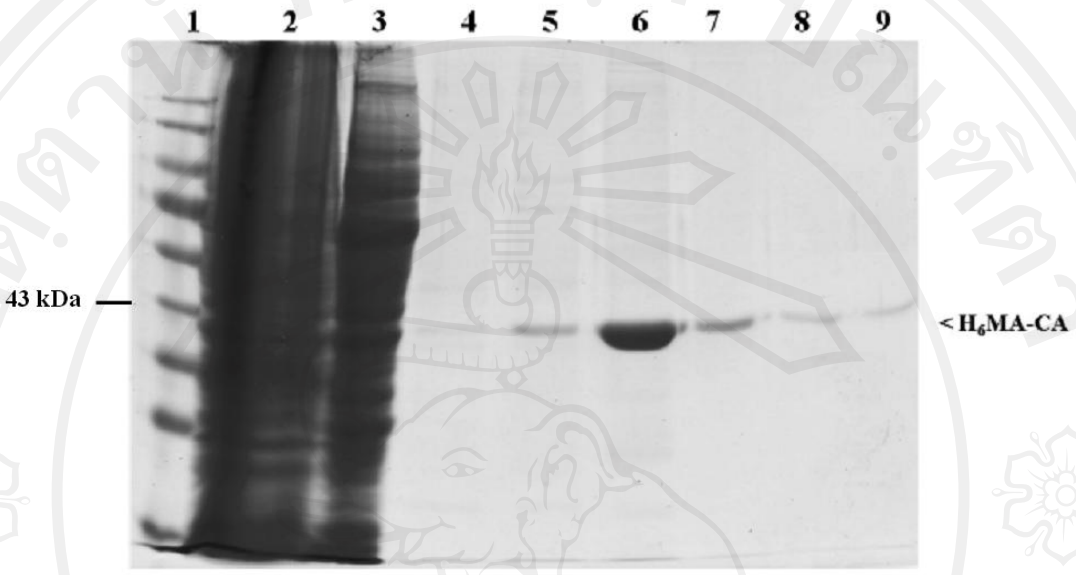

Figure 3.20 Purification of recombinant H_6MA-CA protein using Ni2+-NTA-agarose column. Lane 1, pre-stained protein marker; Lane 2, cell lysate; Lane 3, flow-through fraction; Lane 4-9, eluted fractions. All samples were separated under denaturing conditions in 12% SDS-PAGE. The separated protein in the gel was visualized by Coomassie blue R250 staining.

3.22 Production and characterization of monoclonal antibodies to CA and to MA epitope embedded in H_6MA-CA

To produce a monoclonal antibody to CA, Balb/c mice were immunized with the purified H_6MA-CA, and hybridoma clones were generated using standard hybridoma-generation techniques. After screening and identifying positive clones, a hybridoma clone (designated G18) that produced a monoclonal antibody that was able to bind to the CA domain was identified (see below). The monoclonal antibody produced by clone HB-8975 is known to bind to the C terminus of the MA, and this hybridoma was obtained from the ATCC. The reactivity of both anti-CA mAb G18 and anti-MA mAb HB-8975 was investigated using indirect ELISA. The anti-CA mAb G18 reacted strongly with H_6MA-CA, whereas anti-MA mAb HB-8975 demonstrated no significant interaction **(Fig. 3.21A)**. Based on this result, it appears that anti-MA mAb HB-8975 cannot recognize its MA epitope when embedded in the intact, unprocessed protein, whereas the anti-CA mAb G18 can bind to the CA domain.

The recognition site of both of the above mAbs was validated using Western blotting. The purified H_6MA-CA was incubated with the soluble HIV-PRH_6 fraction to digest H_6MA-CA into the MA and CA domain; the soluble fraction of *E. coli* strain BL21(DE3) or LVS-BL21 was used as a control. As shown in **Figure 3.21B**, recombinant H_6MA-CA, H_6MA, and HIV-PRH_6 were all detected using the anti-His_6 antibody (Lanes 1, 5, and 9, respectively). The anti-CA mAb G18–reactive bands appeared at ~40 kDa and ~24 kDa (Lanes 2, 6, and 10) in the presence and the absence of HIV-PRH_6, respectively. In contrast, the anti-MA mAb HB-8975–reactive

band was only observed when HIV-PRH_6 cleaved the substrate (~17 kDa, Lane 7). Non-specific, endogenous proteases in infected Sf9 cells and LVS-BL21 did not specifically digest at the HIV-PRH_6 cleavage site; therefore, no 17 kDa band was observed in Lane 3 and Lane 11. The results from the indirect ELISA and Western blot analysis indicated that anti-CA mAb G18 bind to both the uncleaved and cleaved forms of the CA domain. By contrast, anti-MA mAb HB-8975 can only react with the proteolytically cleaved H_6MA-CA substrate, a cleaved that exposes its epitope at the free C terminus of MA.

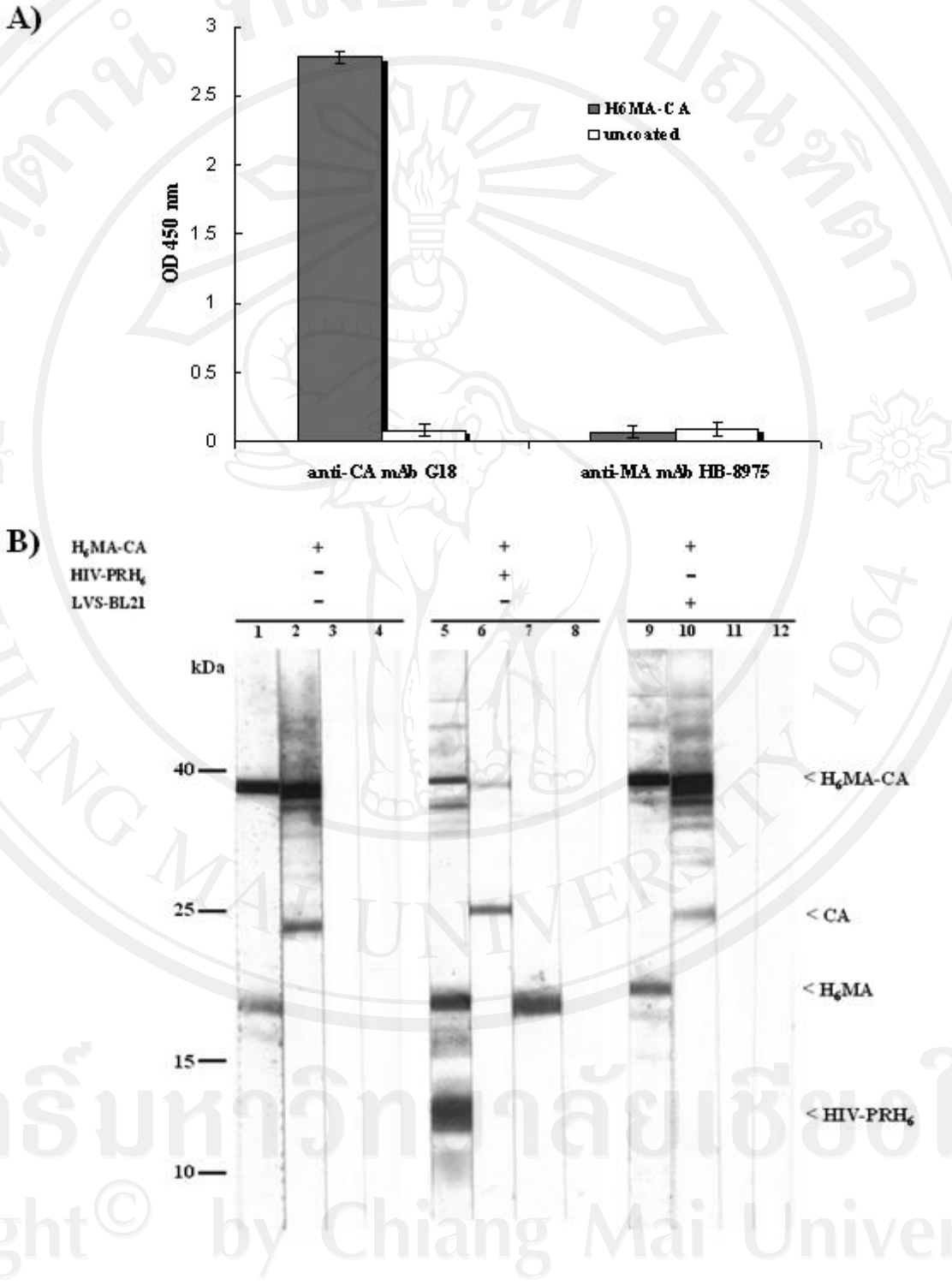

Figure 3.21 Binding of anti-CA mAb G18 and anti-MA mAb HB-8975. **(A)** Two monoclonal antibodies were incubated in H_6MA-CA-coated wells. The captured antibodies were detected using an HRP-conjugated goat anti-mouse immunoglobulin antibody. The white bars represent H_6MA-CA-coated wells, and the grey bars represent uncoated wells. **(B)** Purified H_6MA-CA digested with soluble HIV-PRH_6 or with the soluble fraction of BL21(DE3) (LVS-BL21) was separated and probed with culture supernatants: lanes 1, 5, and 9, anti-His6 antibody; lanes 2, 6, and 10, anti-CA mAb G18; lanes 3, 7, and 11, anti-MA mAb HB-8975; lanes 4, 8, and 12, no antibody. The molecular mass of the recombinant proteins is indicated in kilodaltons (kDa).

3.23 Evaluation of the ELIS-based HIV-PR activity assay (ELIB-PA)

To investigate the efficacy of the ELIB-PA, we measured the HIV-PRH_6 activity using our assay. After the wells were coated with recombinant H_6MA-CA, the soluble HIV-PRH_6 fraction was added. The proteolytic cleavage was carried out under optimal conditions (37°C for 1 hr), and the proteolytic activity of HIV-PRH_6 was detected using specific antibodies (anti-CA mAb G18 and anti-MA mAb HB-8975). As shown in **Fig. 3.2**2, the signal from anti-CA mAb G18 was significantly decreased, whereas the signal from anti-MA mAb HB-8975 was only detected with active HIV-PRH_6. In addition, a protease inhibitor (PI), 1.6 μM of lopinavir (LPV), was used to demonstrate that the reaction occurred *via* HIV-PRH_6 activity. LPV completely abolished the proteolytic activity of HIV-PRH_6. Non-specific proteases from the soluble fraction of *E. coli*, strain BL21(DE3) (LVS-BL21) resulted in a low-

level background cleavage when anti-CA mAb G18 was used as the detection antibody, and there was no significant change detected when anti-MA mAb HB-8975 was used. This suggested that the non-specific proteases did not digest at the HIV-PRH_6 cleavage site. Taken together, these results demonstrated that the proteolytic cleavage of H_6MA-CA occurred as the result of HIV-PRH_6 activity and that non-specific proteases from LVS-BL21 had no effect. Therefore, the ELIB-PA was able to specifically detect the proteolytic activity of HIV-PRH_6.

In addition to the evaluation of the ELIB-PA as a specific assay for HIV-PRH_6 activity, we also used ELIB-PA to examine the proteolytic activity of HIV-PR mutants. To this end, we generated an HIV-PR variant, HIV-PRH_6 I54V, to validate the ELIB-PA with PI-resistant mutant. Compared to signal observed using HIV-PRH_6, when HIV-PRH_6 I54V was used, the change in the anti-CA mAb G18 signal was slightly reduced, and the anti-MA mAb HB-8975 signal was significantly decreased **(Figure 3.22)**. Although the level of expression of HIV-PRH_6 I54V was superior to that of HIV-PRH_6 **(refer to Figure 3.19B)**, its the proteolytic activity was dramatically different. The lower proteolytic activity of HIV-PRH_6 I54V was caused by one amino acid substitution at amino acid residue 54. Additionally, LPV was able to suppress the activity of both HIV-PRH_6 and the I54V mutant. However, even though the mutation of HIV-PRH_6 resulted in decreased activity, the same assay could be used for analysis. Therefore, the ELIB-PA exhibited a high degree of sensitivity in that it was able to detect the proteolytic activity of PR-resistant HIV-PR isolates.

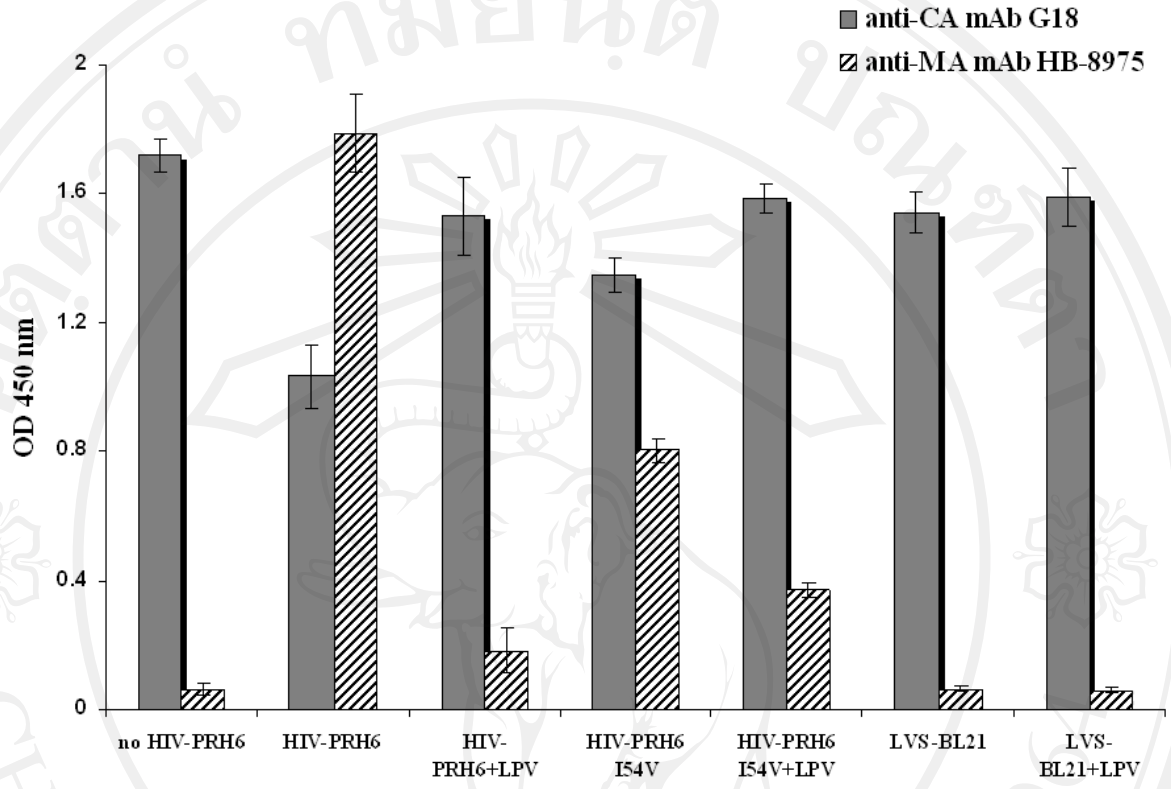

Figure 3.22 Analysis of HIV-PRH$_6$ activity and it variant using the ELIB-PA. The proteolytic activity of soluble HIV-PRH$_6$ based on anti-CA mAb G18 and anti-MA mAb HB-8975 reactivity. The bound antibodies were detected using an HRP-conjugated goat anti-mouse immunoglobulin antibody, and after the addition of substrate and HCl, the signal was measured at 450 nm. The reaction was performed five times. Soluble fractions of BL21(DE3) cells (LVS-BL21) and treatment with lopinavir (LPV) were used to control for non-specific proteases from BL21(DE3) cells and to verify the HIV-PR dependence of the assay, respectively. The proteolytic activity of HIV-PRH$_6$ I54V was compared with the activity of HIV-PRH$_6$ by using ELIB-PA.

3.24 Efficacy and sensitivity of ELIB-PA

HIV-PRH_6 activity was completely abolished in the presence of 1.6 µM LPV. Therefore, to investigate the sensitivity of the ELIB-PA, we determined the half maximal inhibitory concentration (IC_{50}) of LPV and other protease inhibitors, ritonavir (RTV), and nelfinavir (NFV), against HIV-PRH_6. The reverse transcriptase inhibitor, elfavirenz (EFV) was used as negative inhibitor. HIV-PRH_6 was mixed with various concentrations of inhibitors (0-2 µM) prior to measuring the proteolytic activity using the ELIB-PA. As shown in **Figure 3.23A**, the ELIB-PA could generate a dose-response curve and determine the inhibitory effect of each protease inhibitor against HIV-PRH_6. The concentration of all inhibitors at 0.2 µM did not affect proteolysis. Complete inhibition of LPV occurred at 1 µM of LPV, whereas the maximum abolishment of RTV and NFV demonstrated only 60%. Interestingly, the percentage inhibition of RTV and NFV was steady even though the concentration of inhibitors was increased. The EFV presented no inhibition as expected. Using the EILB-PA, the IC_{50} of LPV against HIV-PRH_6 was determined to be 0.6 µM while the IC_{50} of RTV and NEV was 0.8 µM. This result indicated that LPV was the most effective protease inhibitor using ELIB-PA. Furthermore, the inhibition rate of each inhibitor was determined by generating the straight line from the percentage inhibition and the concentrations of inhibitor. The high steep line represented the high acceleration of inhibition. As shown in **Figure 3.23B**, the LPV demonstrated the highest steep line while the inhibition rate of RTV and NFV were less than twice**.** As a consequence, the LPV exhibited the highest affinity compared to others protease inhibitors.

Taken together, ELIB-PA could discriminate between the inhibition efficacy and binding affinity of HIV protease inhibitors by comparing the highest percentage inhibition and IC_{50}. Importantly, the ability to simply generate dose-response curve and determine the IC_{50} will be useful for identifying PI-resistant isolates by observing the reduction in the percentage of inhibition. In addition, determination of drug susceptibility based on the fold change in the IC_{50} will be applicable as a high-through put screening to identify novel PIs for HIV-resistant patients and accelerate the drug discovery process in the pharmaceutical industry.

A)

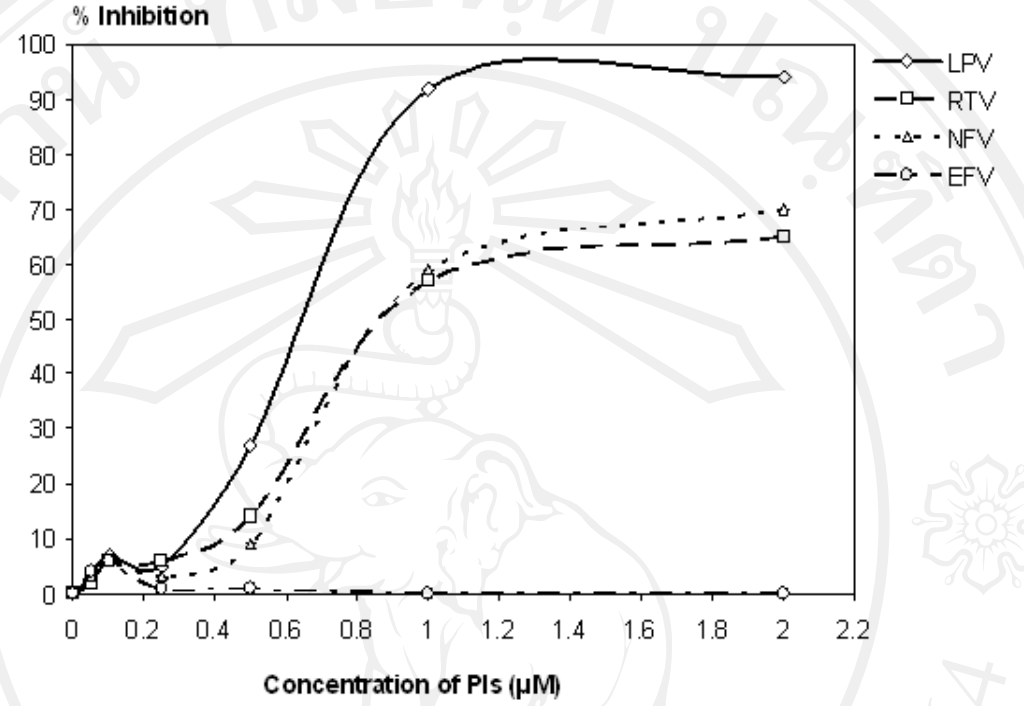

B)

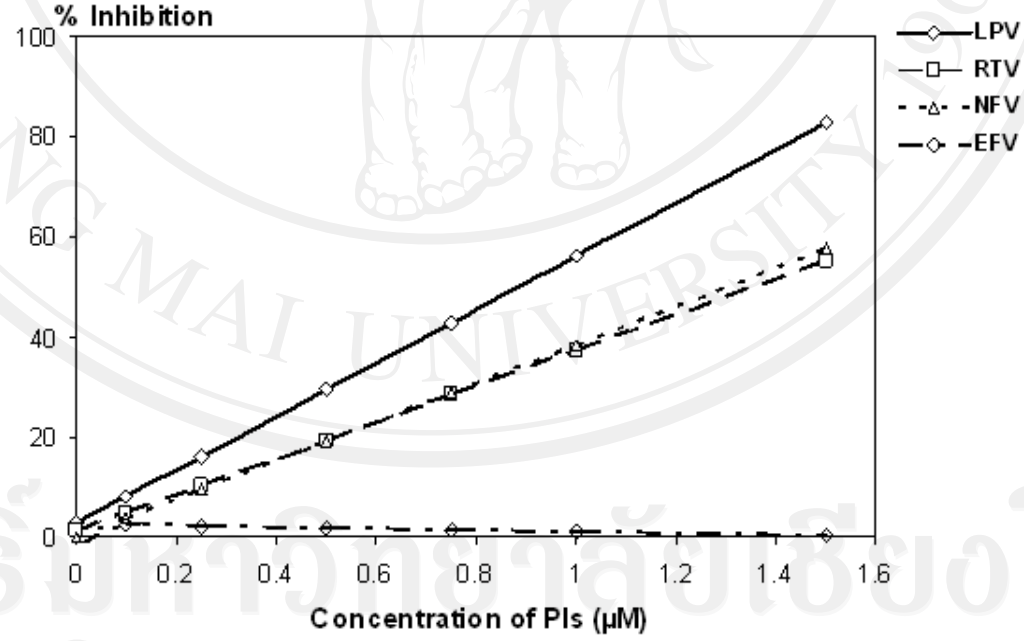

Figure 3.23 Activity of HIV-PRH_6 in the presence of HIV protease inhibitors. (A) Dose-response curve. The relative inhibition of cleavage of H_6MA-CA by HIV-PRH_6 in the presence of the indicated concentrations of each HIV protease inhibitors, LPV (solid line with diamond), RTV (long dashed line with square), and NFV (short dashed line with triangle) is presented. The reverse transcriptase inhibitor, EFV (dashed dot line with circle) was used as negative inhibitor control. The inhibitory effect was evaluated using anti-MA mAb HB-8975. **(B)** Straight line graph**.** The formula on **Figure 3.24A** was used to generate the straight line graph. The derivative of each straight line indicated the affinity and the sensitivity of each inhibitor.